Blade Life Management System for Advanced F Class Gas Turbines

Siemens-Westinghouse W501FC First Stage Nozzle Analysis

1011622

Blade Life Management System for Advanced F Class Gas Turbines

Siemens-Westinghouse W501FC First Stage Nozzle Analysis

1011622

Technical Update, March 2005

EPRI Project Manager
D. Gandy

Electric Power Research Institute (EPRI) • 3412 Hillview Avenue, Palo Alto, California 94304 • PO Box 10412, Palo Alto, California 94303 • USA
800.313.3774 • 650.855.2121 • askepri@epri.com • www.epri.com

DISCLAIMER OF WARRANTIES AND LIMITATION OF LIABILITIES

THIS DOCUMENT WAS PREPARED BY THE ORGANIZATION(S) NAMED BELOW AS AN ACCOUNT OF WORK SPONSORED OR COSPONSORED BY THE ELECTRIC POWER RESEARCH INSTITUTE, INC. (EPRI). NEITHER EPRI, ANY MEMBER OF EPRI, ANY COSPONSOR, THE ORGANIZATION(S) BELOW, NOR ANY PERSON ACTING ON BEHALF OF ANY OF THEM:

(A) MAKES ANY WARRANTY OR REPRESENTATION WHATSOEVER, EXPRESS OR IMPLIED, (I) WITH RESPECT TO THE USE OF ANY INFORMATION, APPARATUS, METHOD, PROCESS, OR SIMILAR ITEM DISCLOSED IN THIS DOCUMENT, INCLUDING MERCHANTABILITY AND FITNESS FOR A PARTICULAR PURPOSE, OR (II) THAT SUCH USE DOES NOT INFRINGE ON OR INTERFERE WITH PRIVATELY OWNED RIGHTS, INCLUDING ANY PARTY'S INTELLECTUAL PROPERTY, OR (III) THAT THIS DOCUMENT IS SUITABLE TO ANY PARTICULAR USER'S CIRCUMSTANCE; OR

(B) ASSUMES RESPONSIBILITY FOR ANY DAMAGES OR OTHER LIABILITY WHATSOEVER (INCLUDING ANY CONSEQUENTIAL DAMAGES, EVEN IF EPRI OR ANY EPRI REPRESENTATIVE HAS BEEN ADVISED OF THE POSSIBILITY OF SUCH DAMAGES) RESULTING FROM YOUR SELECTION OR USE OF THIS DOCUMENT OR ANY INFORMATION, APPARATUS, METHOD, PROCESS, OR SIMILAR ITEM DISCLOSED IN THIS DOCUMENT.

ORGANIZATION(S) THAT PREPARED THIS DOCUMENT

Turbine Technology International, Inc.

This is an EPRI Technical Update report. A Technical Update report is intended as an informal report of continuing research, a meeting, or a topical study. It is not a final EPRI technical report.

ORDERING INFORMATION

Requests for copies of this report should be directed to EPRI Orders and Conferences, 1355 Willow Way, Suite 278, Concord, CA 94520, (800) 313-3774, press 2 or internally x5379, (925) 609-9169, (925) 609-1310 (fax).

CITATIONS

This report was prepared by

Turbine Technology International, Inc.
2024 West Henrietta Road, Suite 5F
Rochester, New York 14623

Principal Investigators
E. Wan,
C. Hong
R. Dewey

This report describes research sponsored by the Electric Power Research Institute (EPRI).

The report is a corporate document that should be cited in the literature in the following manner:

Blade Life Management System for Advanced F Class Gas Turbines: Siemens-Westinghouse W501FC First Stage Nozzle Analysis, EPRI, Palo Alto, CA: 2005. 1011622.

REPORT SUMMARY

This report is a continuation in an ongoing series of life management studies for turbine hot section components. It represents the efforts associated with benchmarking the 1st row nozzle of the Siemens-Westinghouse 501F (5000F) class of machines. It describes the application of the Hot Section Life Management Platform (HSLMP) and the temperatures and stress that occur in the nozzle during normal base load operation.

Background

The HSLMP was developed by EPRI as a means to examine in detail features of the engineering and durability as required to support the management and monitoring of these components. The platform was developed to provide a consistent, objective third-party system by which independent information on life consumption and coating degradation can be made available to operators for making practical decisions regarding their newest generation of gas turbines.

Objectives

The specific objective for this evaluation was to successfully run an aero thermal analysis of the SW 501 1st stage nozzle in order to benchmark the temperatures and stress produced in the component at base load operation. Results were to be correlated against known conditions of degradation observed in serviced parts.

Approach

In support of this initial application of the HSLMP to a nozzle, the team correlated results obtained from airflow measurements tests on an actual nozzle, and against field reports of fatigue and oxidation published on these parts. As a product of the application, the methodology was successfully developed as a critical part of the overall procedure that would be used for a transient thermal analysis and/or to examine other nozzles operated in a turbine hot section.

Results

Thermal-mechanical fatigue plays a primary role in determining the ultimate durability and longevity of the W501FC 1st stage blade. Creep also contributes to the cracking occurring near the platform cooling hole. Both damage mechanisms were attributed to thermally induced stresses resulted from pronounced temperature gradients observed in the results. The effect of TGO growth on potential de-lamination or spallation of TBC appears less significant as compared to the damage caused to the 1st stage-rotating blade. However, bond coat oxidation might become a more critical factor under long-term service.

EPRI Perspective

Advanced simple cycle combustion turbines and combined cycle machines dominate the new generation marketplace. These machines rely on superalloy cast components protected by coating systems and complex cooling passage arrangements. In terms of temperature and stress, the first stage nozzle is subject to the harshest operating environment. Initial field experience has raised concerns about component durability, prompting development of a detailed aero-thermal stress model. This evaluation is one of a continuing series of studies focused on the life assessment and management of F-Class of combustion turbine components.

Keywords

Gas turbines
Combustion turbines
Operators
Maintenance
Turbine Life Management

ABSTRACT

This report documents the application of the HSLMP to provide a benchmark or baseline of the temperatures and stresses of the SW W501FC 1st stage nozzle. A rigorous program of aero-thermal modeling was undertaken to simulate the complicated internal and external cooling configuration of the hot section component. An airflow test was also performed to verify and refine the cooling flow model critical to the overall process. Results from the aero-thermal analysis were used to evaluate the bulk metal temperature within the 1st stage nozzle. Overall, the results show sufficient cooling is achieved by a combination of the advanced cooling path configuration and TBC system of protection. Externally however, high temperature gradients were predicted in localized regions of the airfoil and shroud. It is believed that reports of cracking at the juncture between the inner shroud and vane is a consequence of thermal cycling, and caused by the thermal stress induced from this high temperature gradient. Localized stresses were also predicted to occur near the hub of each of the three cavities that form the nozzle vane, with a maximum stress concentration occurring near the 3rd cavity. The resulting patterns of stress were found to conform to the thermal gradient across the wall and along the fillet radii. The geometric transition from the vane airfoil to the shroud further contributes to the overall stress occurring within the inner shroud-fillet region.

CONTENTS

1 PROGRAM OBJECTIVES 1-1
1.1 Objectives and Approach 1-1
1.2 Features and Degradation Modes of the W501FC 1st Stage Nozzle 1-5

2 AERO THERMAL ANALYSIS 2-1
2.1 Throughflow Analysis 2-1
2.2 Internal Cooling Flow Analysis 2-4
2.3 External Flow Analysis 2-8

3 VERIFICATION OF INTERNAL COOLING 3-1
3.1 Test Design 3-1
3.2 Test Methodology 3-2
3.3 Exit Hole Mapping 3-5
3.4 Summary of Flow Measurements 3-6
3-5 Correlation of CPF Results with Air Flow Results 3-8
3.6 Summary of Test Results 3-11

4 THERMAL ANALYSIS 4-1
4.1 Finite Element Model 4-1
4.2 Steady State Results 4-3

5 STRESS ANALYSIS 5-1
5.1 Stress Results 5-1

6 CONCLUSIONS 6-1

7 SUMMARY REMARKS 7-1
References 7-4

LIST OF FIGURES

Figure 1-1 W501FC 1st Stage Nozzle Identifying Different Cooling Strategies 1-3
Figure 1-2 W501FC 1st Stage Nozzle Chambers and Core Plugs 1-6
Figure 1-3 Examples of Damage Found on W501FC 1st Stage Nozzles 1-7
Figure 2-1 Radial Profile of Temperature Ratio at Turbine Inlet 2-2
Figure 2-2 Radial Profile of Absolute Temperature at Full Load Condition................................2-3
Figure 2-3 Cooling Flow at Mean-Diameter Branched Passages of First Channel....................2-7
Figure 2-4 Cooling Flow at Mean-Diameter Branched Passages of Second Channel 2-7
Figure 2-5 CFD Mesh at Flow Path of Mean Section 2-9
Figure 2-6 Static Pressure and Mach Number Distribution...2-10
Figure 2-7 Variation of Film Coefficient Predicted at Mean Diameter 2-11
Figure 3-1 Compressor and Regular Used in Airflow Test 3-2
Figure 3-2 Third Cavity Manifold...3-3
Figure 3-3 First Cavity Manifold 3-3
Figure 3-4 Probe Tips and Assembly of Mass Flow Sensor & Probe 3-4
Figure 3-5 Probe on Cooling Orifice and Data..3-5
Figure 3-6 Referenced Exit Holes on Suction and Pressure Side of Airfoil 3-5
Figure 3-7 Numbering of Exit Holes at Outer and Inner Flange of Third Cavity.........................3-6
Figure 4-1 Element and Surface Plots of the W501FC 1st Stage Nozzle FE Model...................4-1
Figure 4-2 Physical and Mechanical Properties of Mar-M509 4-2
Figure 4-3 Predicted Temperature Distributions for W501FC 1st Stage Vane............................4-3
Figure 4-4 Predicted Temperature Distributions of TBC Layers 4-4
Figure 4-5 Predicted Cooling Effectiveness..4-4
Figure 4-6 Temperature Distribution for TBC Coated Nozzle Using Different Base Metals.......4-5
Figure 4-7 Predicted Temperature Distributions near Inner Fillet Region.................................4-5
Figure 5-1 Equivalent Stress Distribution of 1st Stage Nozzle 5-1
Figure 5-2 Radial Stress Distribution in Base Metal 5-2
Figure 5-3 Minimum Principal Stress Distribution of Base Metal 5-3

LIST OF TABLES

Table 1-1 Cooling Hole Distributions of W501FC 1st Stage Nozzle 1-3
Table 1-2 Performance Parameters and Design Life for W501FC 1st Stage Nozzle.................. 1-5
Table 1-3 Conversion Formulations Used In Report... 1-8
Table 2-1 Hub and Tip Diameters Used to Define Hot Gas Path 2-2
Table 2-2 Throughflow Results – First Stage Nozzles at Full Load Operation 2-4
Table 2-3 Steady-State Cooling Flow Distribution 2-6
Table 2-4 Averaged Temperature and Film Coefficients of Third Channel................................ 2-8
Table 3-1 Summary of Measured Air Flow at Various Supply Pressures 3-6
Table 3-1 Summary of Measured Air Flow at Various Supply Pressures (Continued) 3-7
Table 3-2 Air Flow Comparison of First Cavity 3-8
Table 3-3 Air Flow Comparison of Second Cavity 3-9
Table 3-4 Air Flow Comparison of Third Cavity 3-10

1
PROGRAM OBJECTIVES

1.1 Objectives and Approach

The durability of combustion turbine first stage nozzles is always of particular relevance to managing maintenance, operating and life cycle costs since these parts are exposed to the highest gas temperatures in the hot gas path section. Oxidation, creep and thermal mechanical fatigue (TMF) are the principle forms of degradation, driven by the temperatures and stresses that are produced in this extreme of the operating environment. Cracking, induced by thermal stress during cycling, is the primary cause typically reported as accountable for the repair and fallout rates of these particular components.

The design engineering of the 1st stage nozzle is always a further concern whenever the firing temperature is raised for a class of turbines to increase the unit output and improve overall cycle performance. Improvements, including thermal barrier coatings (TBC), are the latest in the front line of defenses developed to counter these increases, and mitigate any acceleration in their degradation. Design enhancements have also been rigorously employed to promote the most efficient use of the cooling flow made available to the nozzle.

As a result of these improvements in coating and cooling strategies, the overall bulk metal temperatures for these critical components has generally been maintained below the allowable limits of the base metals. However, cracking continues as a predominant failure mode of nozzles operated in the most advanced F-class machines. These nozzles often require either expensive repairs to restore their durability or face premature retirement and replacement. Significant cracking typically occurs in the vane and sidewall areas. Often both numerous and long, these cracks are visible on the exterior surfaces. Reported field experience further suggests that such major cracks initiate very early in the service life cycle of the nozzle then propagate at a slower rate as the thermal stress is relieved during the process of cracking. This cracking is presently believed as primarily driven by Low cycle fatigue/Thermal mechanical fatigue (LCF/TMF) from thermal cycles during the start-up and shutdown of the unit. [1]

Time-dependent damage such as creep is also believed to contribute significantly to initiation and propagation of cracks. In nozzle cracking time-dependent issues are recognized as involving a number of complicated technical issues:

- Changes in the microstructure from prolonged exposure to high temperatures may lead to an increase of hardness. This could result in a loss in ductility and a decrease in low cycle fatigue strength.

- Environmental attack near the crack tip region could accelerate its propagation and embrittle the cobalt-based superalloys used in the nozzle.
- Oxidation within the shroud area remains a particular issue for nozzles operated in base load machines.
- Erosion, FOD and plugging of cooling holes are other time-related modes of damage and degradation that often affect the 1st stage nozzles.
- Hot spots, due to a non-uniform gas temperature profile in the circumferential direction, could also present problems to certain designs.

While cracking of the 1st stage nozzle is therefore critical, as it can ultimately control or dictate the timing of the overall hot gas path inspection, it is still often treated as an inherent maintenance problem and not a design issue.

Although modifying the design might appear as the more effective approach to correct localized cracking, the aero-thermal and stress analyses of a vane segment with a TBC and advanced cooling system is a highly complicated and difficult process to simulate. In lieu of aero thermal modeling, measures used to date to extend the life of a particular design have principally relied on a combination of field inspection, measurement and data collection. Prediction of crack growth rates by OEMs or repair vendors is more likely to be based on historical statistics in order to estimate the remaining life of a cracked nozzle and define crack limits to avoid catastrophic failure [2], [3]. Such limits though, are essentially based on engineering judgment, or what sometimes appear to be convenient associations. For example in reference [2], rather than undertake a sophisticated fracture mechanics study, the sidewall axial length and airfoil chord length were simply used to assign limits to the length of sidewall cracks and airfoil cracks, respectively.

As an alternative to this trial and error approach for establishing inspection intervals and damage limits, one of the purposes of this examination was to demonstrate the feasibility of performing a basic design audit of a nozzle, despite the many technical obstacles. The S-W 501FC 1st stage was selected as a representative candidate with features typically shared among F-class designs. The analysis of the thermal and stress response of a modern 1st stage nozzle proved extremely challenging, if not unprecedented. Starting with geometry, there are a total of 767 cooling holes in the S-W 501FC nozzle: 677 in the airfoil, 52 in the outer shroud and 38 in the inner shroud **(Table 1-1)**. To accurately represent the critical effect of the cooling flow throughout the entire structure, each of these passages must be explicitly represented in the model. The addition of a TBC system where multiple layers of elements represent the complete system of the TBC to bond coat adds a further complication to the model **(Figure 1-1)**.

Because an aero thermal solution was the ultimate objective, a brute force approach of relying on the finite element program to auto-mesh volumes and construct the nozzle model was not considered as feasible. If an excessive number of randomly assigned elements are used to represent the structure and coating system, the computational time required for manipulating the enormous amounts of thermal boundary conditions in concert with a large finite element model becomes unrealistically long. Even if such a single brute force solution could be successfully achieved, the ability to make multiple runs of transient operating conditions, or to use the model to parametrically examine design repairs or limited modifications would become impractical if not impossible.

Table 1-1
Cooling Hole Distributions of W501FC 1st Stage Nozzle

Shower Head- Leading Edge	138
Film Cooling – Suction Side	242
Film Cooling – Pressure Side	267
Pin Fin Slot – Trailing Edge	30
Outer Shroud Cooling	52
Inner Shroud Cooling	38
Total # of Holes	767

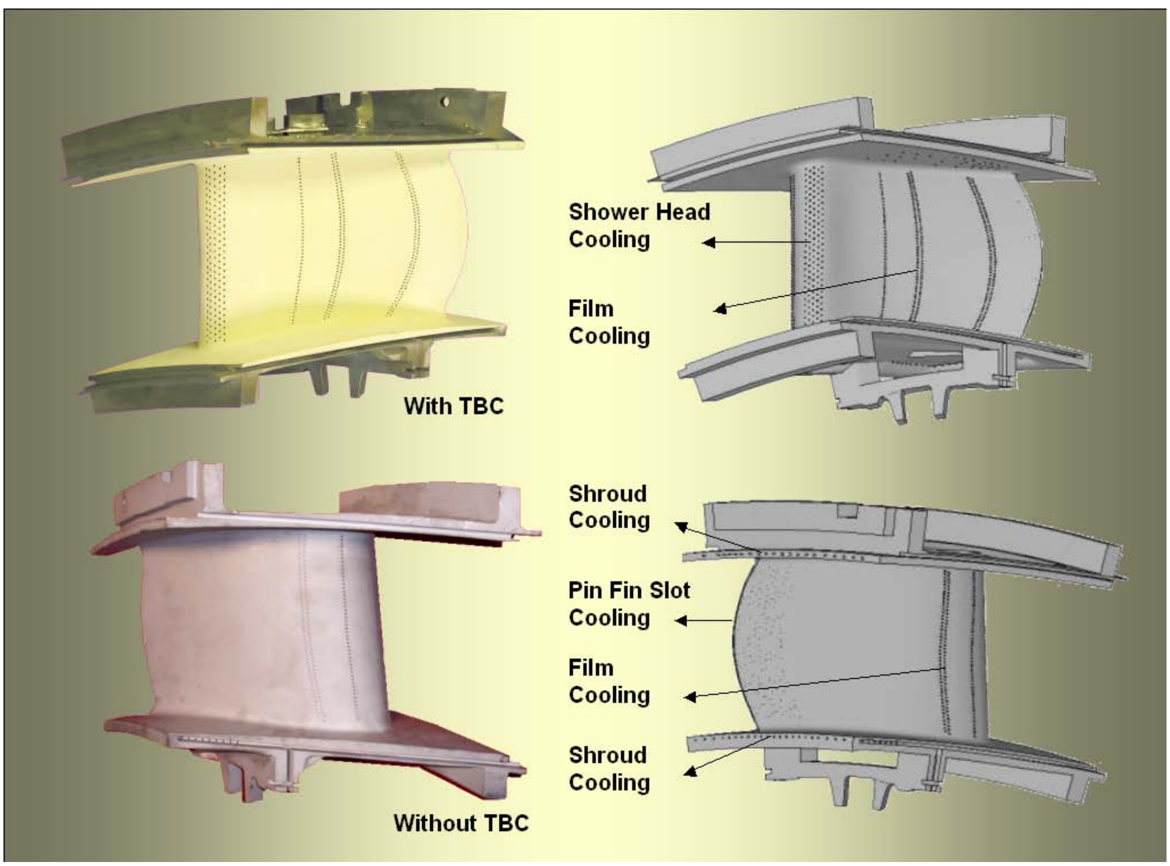

Figure 1-1
W501FC 1st Stage Nozzle Identifying Different Cooling Strategies

Since a fundamental purpose of the HSLMP is to be able to audit the design characteristics of any selected hot section component, a premium is placed on being able to obtain a solution within a reasonable run-time. In the case of the 501FC nozzle, as with its rotating blade counterpart, the final model was carefully designed with a highly structured grid work of systematically defined and organized elements. Even so, this particular model consisted of over 100,000 elements and took several man-months to construct.

Pursuant to this approach, nozzle geometry was first obtained by reverse engineering samples made available to support the aero-thermal modeling. A sample nozzle was partially cut apart to obtain details of the internal structure. Since this represented an initial application of the HSLMP to such a nozzle, a comprehensive airflow test was also performed on an intact component. The objective of testing was to document and characterize the behavior of the cooling flow with core plugs inserted within the nozzle cavities. The results provided a basis to guide and verify the aero thermal models subsequently used to perform the benchmark analysis.

As with the 1st stage rotating blades, the overall simulation relies on two basic types of models: (1) aero-thermal models provide the external heating, internal cooling and heat conduction, (2) structural models provide details on the stresses and strains produced as a consequence of the balance between internal and external thermal loads. External flow was modeled using a computational fluid dynamics (CFD) program developed by NASA. Internal cooling flow was modeled using customized version of the NASA Cooling Passage Flow (CPF) program.

The final technical scope of work involved systematic completion of the following sub-tasks:

1. Reverse engineering of 1st stage nozzle.

2. Airflow testing on all three cavities with impingement covers and core plugs attached.

3. Preparation of the finite element based computer model of the 1st stage nozzle.

4. Performance of a through-flow analysis to characterize the governing aero-thermal parameters at the inlet and exit of the stationary stage.

5. Performance of external gas flow and heat transfer analysis to calculate heat transfer coefficients around the airfoil profile.

6. Performance of an internal cooling flow and heat transfer analysis to calculate the cooling air temperature and heat transfer coefficients occurring along the entire cooling flow passages.

7. Performance of a steady state thermal analysis by applying the boundary conditions required for all the cooling holes.

8. Performance of a steady stage stress analysis to identify critical locations and resulting stress distributions at base load operating conditions.

Traditionally, the HSLMP is used to study the response of a hot section component design for both steady state (base load) and transient thermal (peaking) operating conditions. Given the modeling challenges previously listed, the immediate study was therefore limited to an aero thermal analysis of the nozzle during base load operation. Once it could be demonstrated that a reasonable solution was possible for such a highly complex structure, performing a transient solution should be technically feasible. To complete such a solution, the remaining challenge would shift from constructing the model to effectively processing the enormous amount of data that is involved when the transient thermal load is broken down into a sequence of time steps and solved iteratively until a steady state condition is arrived upon.

1.2 Features and Degradation Modes of the W501FC 1st Stage Nozzle

The S-W W501FC is a 3600-RPM combustion turbine, which presently operates at a firing temperature of about 2400º F (1316º C) exiting the 1st stage nozzle. The average turbine inlet temperature entering the 1st stage nozzle is estimated to be about 2534º F (1390º C). **Table 1-2** lists the performance parameters and design life for the 1st stage nozzle. The target design life for repair and replacement is currently 800/1600 equivalent starts (ES) and 16,000/48,000 equivalent operating hours (EOH), respectively. The 1st stage nozzles are precision cast of Cobalt base alloy ECY768, and coated with a TBC.

Table 1-2
Performance Parameters and Design Life for W501FC 1st Stage Nozzle

Output (MW)	Pressure Ratio	Net Efficiency (%)	Repair (EOH/ES)	Replace (EOH/ES)
171	15	36.5	16,000/800	48,000/1600
EOH – equivalent operating hours; ES – equivalent number of starts				

The 1st stage features 32 single-vane segments. The single vanes are removable. They are supported by an individual inner casing that is keyed to allow an axial and radial thermal response of the vane segments. Theoretically, a single-vane segment design has the benefit of reducing stresses near the airfoil-shroud junctions, in comparison to a three-vane segment design [4]. Nevertheless, the appearance of significant cracks near the inner shroud and airfoil fillet radii region have been identified for the W501FC 1st stage nozzle.

The nozzle utilizes three impingement inserts (core plugs) in conjunction with arrays of film cooling holes and a trailing edge pin fin system (**Figure 1-2**). The leading and middle cavities take air discharged directly from the compressor. The aft cavity utilizes spent shroud cooling air. A showerhead film cooling arrangement on the leading edge, and arrays of film cooling on both the pressure and suction sides of the airfoil, are used to further enhance the overall cooling provided to the nozzle.

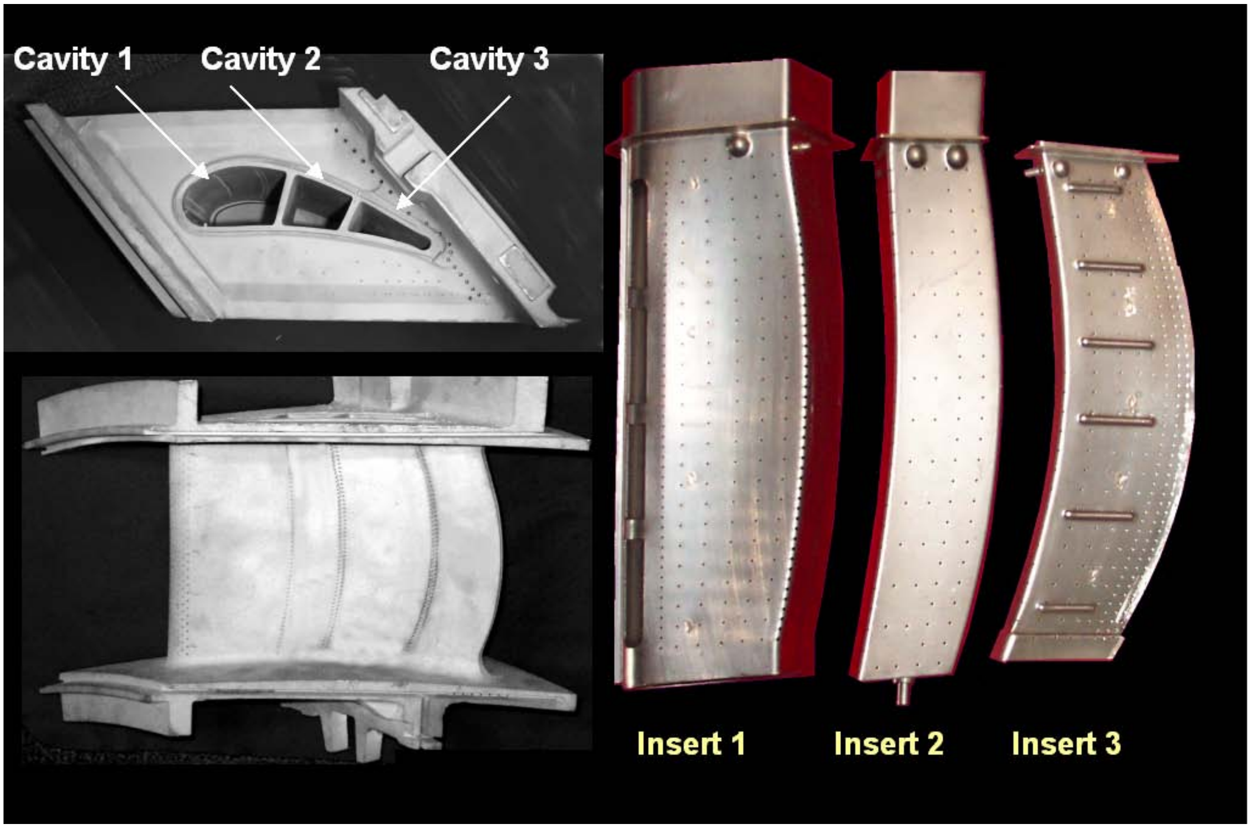

Figure 1-2
W501FC 1st Stage Nozzle Chambers and Core Plugs

Cracking in the fillet region near the inner shroud-airfoil juncture presently appears to be a significant life limiting mode of degradation for the W501FC 1 stage nozzle design **(Figure 1-3)**. Cracking at the inner fillet originates around the trailing film cooling holes found on the pressure side. These then extend either toward the leading edge or continue to proceed up through the row of holes. This pattern is sometimes described as "zipper" cracking.

On a sample nozzle with a history of approximately 150 starts, the length of the inner fillet crack was measured and found to exceed 11.0" (279 mm), or well beyond the allowable repair limit. Numerous cracks were also observed at other arrays of film cooling holes on the pressure side. Inner shroud cracking was present at the edge propagating into fillet area near the mid-span on suction side. Cracking in the outer shroud was detected at the trailing edge on the suction side. The cracks in the outer shroud and inner shroud sidewall region were not as visible and much less severe than those observed in the vane and fillet regions.

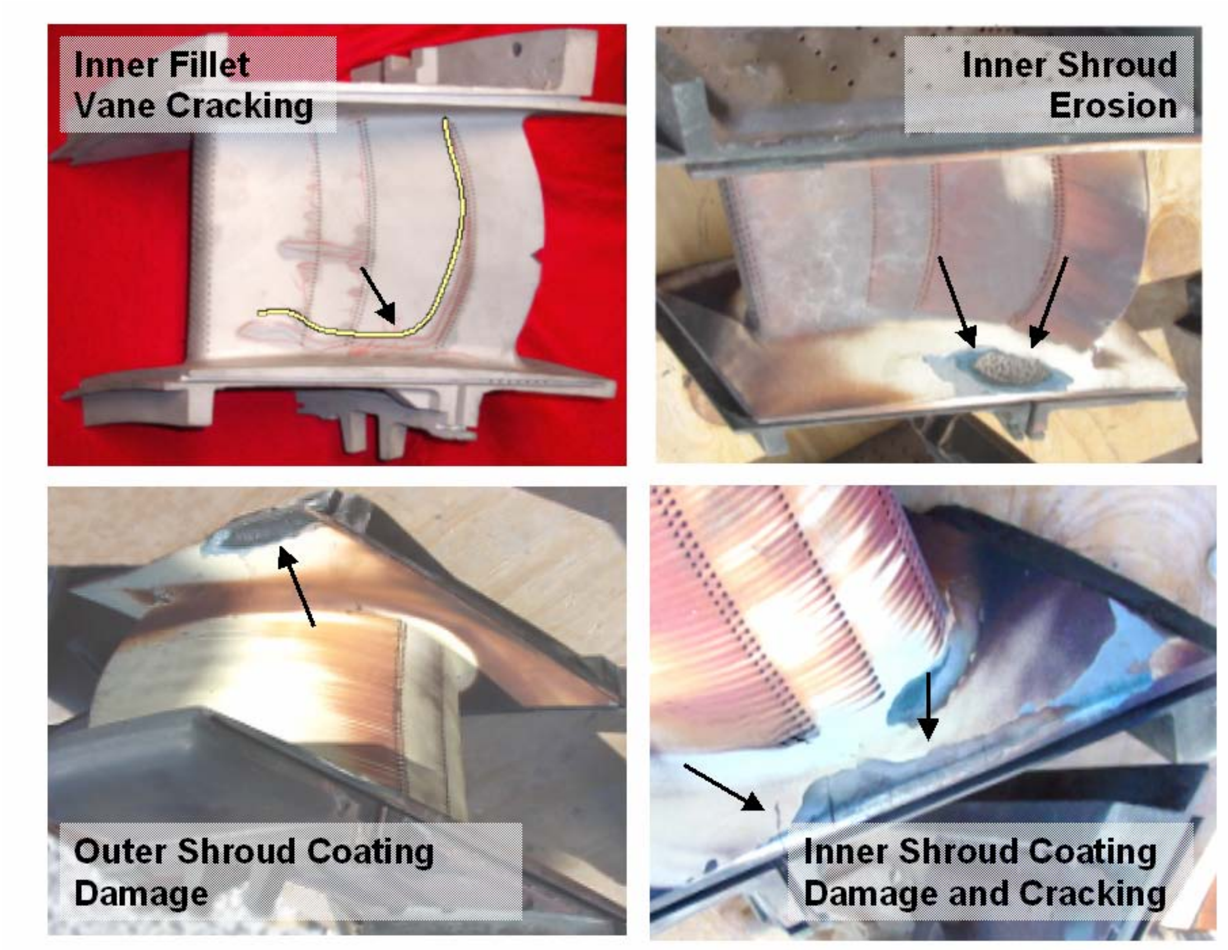

Figure 1-3
Examples of Damage Found on W501FC 1st Stage Nozzles

As shown in **Figure 1-3**, coating damage on the outer shroud near the trailing edge has also been observed along with erosion damage on the pressure side of the inner shroud. The pattern of multiple cracks observed firsthand is consistent with other field reports. This would indicate that the problem is an inherent issue related to the nozzle design, and primarily due to thermally driven low cycle fatigue. The more severe cracking at the juncture of the inner shroud and vane on the pressure side is likely to be the most critical location of damage, as it could lead to the liberation of metal and subsequent damage to the components downstream.

In conjunction with the physical requirements previously cited, it was therefore necessary to ensure that the aero-thermal model would reasonably characterize the temperatures in this region and produce stress distributions that would be consistent with the damage observed from the serviced parts.

Since both English and SI units are used extensively throughout the remainder of this report, conversions made to SI units are in accordance to **Table 1-3**.

Table 1-3
Conversion Formulations Used In Report

Operating Condition	Table Head
Temperature	1 degree F = (X-32) x 5/9 degrees C
Psi / ksi	1 phi = 0.006895 Mpa, 1 ksi = 6.895 Mpa
Inch	1 inch = 25.4 mm
Pound	1 lb = 0.4539 kg
Heat Transfer Coefficient	1 Btu/ft^2-°F-s = 20441.5 W/m^2-°C

2
AERO THERMAL ANALYSIS

2.1 Throughflow Analysis

To perform the aero-thermal portion of the overall HSLMP analysis, global boundary conditions were first obtained to determine the film coefficients and bulk temperatures acting on the internal and external surfaces of the nozzle. A throughflow analysis of the entire turbine gas path was performed to obtain a radial distribution of both the aerodynamic and thermodynamic parameters at the inlet and exit of each stage. The total pressure, temperature and flow angles provided by the model are then used as input to a more refined CFD model of the primary gas flow and internal cooling flow around the nozzle.

To set up a throughflow model, the flow field of a multi-stage hot gas path is divided into an annulus region and the individual blade-to-blade regions. A customized program is applied, which was specifically designed to analyze the annulus region between stationary and rotating rows of a gas turbine. Customization included the incorporation of specific algorithms to deal with (1) temperature and/or pressure profile at the turbine inlet, (2) mixing between the cooling flow and main gas flow, and (3) potentially arbitrary mass flow rates and inlet/outlet conditions.

The annulus region of W501 FC gas turbine was defined by the hub and tip diameters of the four stationary and rotating rows, as shown in **Table 2-1**. At full load (180 MW), the boundary conditions input to the model include a firing temperature of 2,400°F (1,316°C) at the exit of first nozzles, a turbine exhaust temperature of 1,090°F (588°C), and a turbine exhaust pressure of 15.0 psia (0.103 Mpa).

Other relevant parameters also required as input are itemized as:

- The radial profile of the temperature ratio at the turbine inlet **(Figure 2-1)**.
- The mass flow rate at each stage starting from upstream to downstream: 2.65×10^6 lbm/sec (1.20×10^6 kg/sec), 3.08×10^6 lbm/sec (1.40×10^6 kg/sec), 3.23×10^6 lbm/sec (1.47×10^6 kg/sec), 3.23×10^6 lbm/sec (1.47×10^6 kg/sec).
- The radial clearance of the seals, assumed as approximately 0.02 inch (0.051 cm).
- The mass flow, temperature and pressure within the cooling passages. These were either estimated or calculated using CPF.

Table 2-1
Hub and Tip Diameters Used to Define Hot Gas Path

		Inlet Hub Diameters	Inlet Tip Diameters	Exit Hub Diameters	Exit Tip Diameters
Stage 1	Nozzle	66.61 inch (169.2 cm)	79.70 inch (202.4 cm)	66.61 inch (169.2 cm)	79.70 inch (202. 794 cm)
	Blade	66.61 inch (169.2 cm)	79.70 inch (202.4 cm)	66.50 inch (168.9 cm)	79.70 inch (202.4 cm)
Stage 2	Nozzle	65.00 inch (165.1 cm)	82.01 inch (208.3 cm)	63.96 inch (162.50 cm)	82.98 inch (210.8 cm)
	Blade	63.50 inch (161.3 cm)	83.50 inch (212.1 cm)	62.70 inch (159.3 cm)	85.40 inch (216.9 cm)
Stage 3	Nozzle	62.04 inch (157.6 cm)	88.95 inch (225.9 cm)	60.96 inch (154.8 cm)	91.50 inch (232.4 cm)
	Blade	60.60 inch (153.9 cm)	92.30 inch (234.4 cm)	59.30 inch (150.6 cm)	94.90 inch (241.0 cm)
Stage 4	Nozzle	57.80 inch (146.8 cm)	98.02 inch (249.0 cm)	56.85 inch (144.4 cm)	101.5 inch (257.8 cm)
	Blade	56.41 inch (143.3 cm)	102.8 inch (261.1 cm)	55.10 inc (140.0 cm)	104.9 inch (266.4 cm)

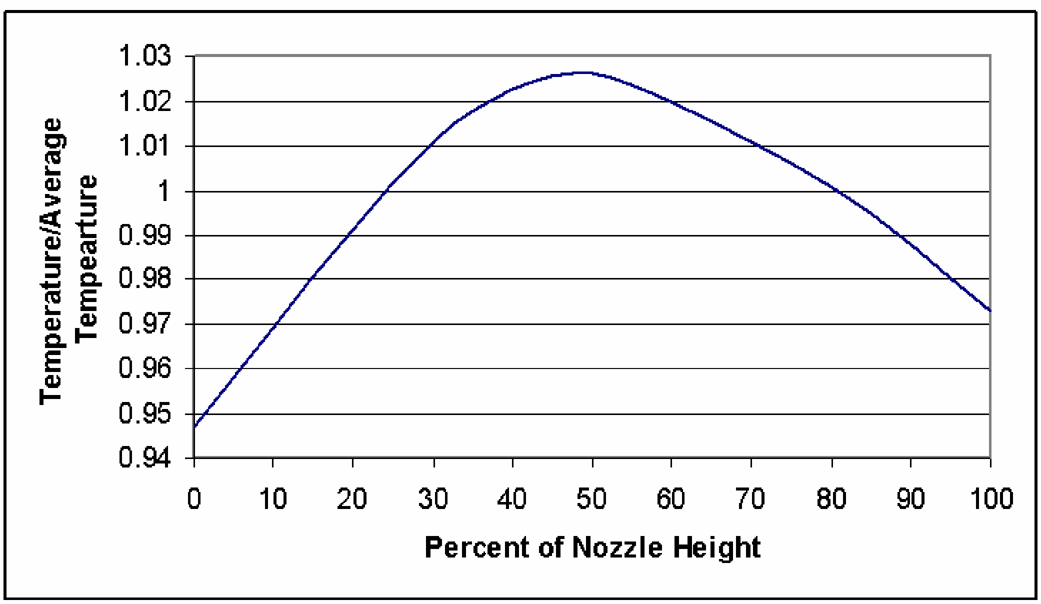

Figure 2-1
Radial Profile of Temperature Ratio at Turbine Inlet

By means of an iterative process, the efficiency of each stationary and rotating row is adjusted until the results converge to be equivalent with the specified overall (global) boundary conditions. At the completion of the analysis, the radial distribution of both aerodynamic and thermodynamic parameters at the inlet and exit of each row is provided as an output file.

For the W501FC unit, the turbine inlet pressure was computed to be 218 psia (1.503 MPa), or slightly less than the compressor discharge pressure of 224 psia (1.544 MPa), accounting for the loss occurring between compressor discharge and turbine inlet. As a byproduct of the analysis, the gross shaft power generated by the combustion turbine was calculated as 303 MW (71 MW produced from the first stage, 69 MW from the second stage, 62 MW from the third stage and 101 MW from the last stage.

The radial profiles of absolute temperature at the inlet and the exit of each turbine stage are shown in **Figure 2-2,** with respect to a full load operating condition. The average turbine inlet temperature was found to be 2,534^{o} F (1,390^{o} C). The computed average temperature at the exit of last stage was 1,120^{o} F (604^{o} C), or 30^{o} F (17^{o} C) greater than the turbine exhaust temperature to account for the loss occurring at the exhaust. It is noted that the radial profile of absolute temperature at each stage is influenced by a number of factors. These include the profile at turbine inlet, the efficiency of streamlines, the seal configurations and clearances, and the mix of cooling flow with main gas flow. As a consequence of these factors, the radial profile at the exit of the last stage becomes relatively flat.

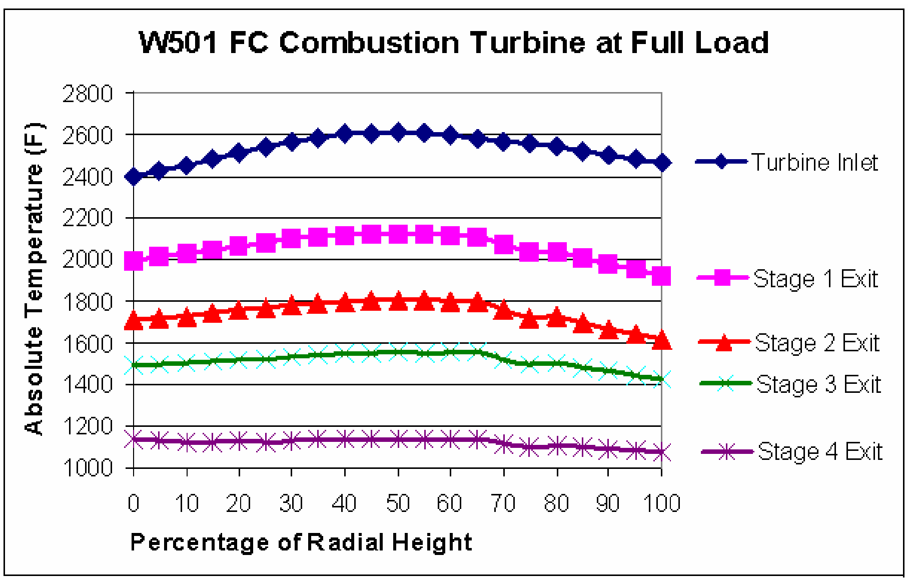

Figure 2-2
Radial Profile of Absolute Temperature at Full Load Condition

The throughflow results for the 1st stage nozzles are listed in **Table 2-2**. The maximum temperature at the turbine inlet is calculated as 2,611^{o} F (1,433^{o} C). The inlet total pressure was calculated to be 218 psia (1.503 MPa) for an idealized uniform distribution from hub to tip. A zero degree of inlet flow angle indicates that the gas flow coming out from the combustor is in the axial direction. The exit static pressure increases from 153 psia (1.055 MPa) at the hub to 168 psia (1.158 MPa) at the tip. These parameters served as the boundary conditions for the subsequent internal cooling flow and external flow analysis.

Table 2-2
Throughflow Results – First Stage Nozzles at Full Load Operation

Height (Percent)	Inlet Total Temperature	Inlet Total Pressure	Inlet Flow Angle	Exit Static Pressure
0 (Hub)	2,394 °F (1,312 °C)	218 psia (1.503 MPa)	0°	153 psia (1.055 MPa)
25	2,542 °F (1,394 °C)	218 psia (1.503 MPa)	0°	156 psia (1.076 MPa)
50 (Mean)	2,611 °F (1,433 °C)	218 psia (1.503 MPa)	0°	159 psia (1.096 MPa)
75	2,556 °F (1,402 °C)	218 psia (1.503 MPa)	0°	163 psia (1.124 MPa)
100 (Tip)	2,394 °F (1,352 °C)	218 psia (1.503 MPa)	0°	168 psia (1.158 MPa)

2.2 Internal Cooling Flow Analysis

To complement the throughflow analysis, the NASA cooling passage flow (CPF) program [5] is used to analyze in detail the internal cooling flow of a selected component. CPF integrates the one-dimensional compressible momentum equation and energy equation along a defined flow path. Along this path, it accounts for the effects of area changes, mass additions or subtractions, pumping, friction, and wall temperature effects. Flow may also be bled off to represent tip cap impingement as well.

CPF calculates mass flow rate, temperature, pressure, velocity and the film coefficients along the various types of channels used in advanced hot section components to promote turbulence.. These can include roughened plain passages, pin-fin passages, finned passages and trip-strip passages. In addition, the original CPF program was refined to deal with complex configurations of branched passages and multiple impingement cooling passages featured in the F-class generation of units. As part of the overall process of analysis, the computed gas temperatures and film coefficients are eventually supplied to the finite element heat conduction model of the 1st stage nozzles together with relevant external flow solutions in order to calculate the metal temperature distributions throughout the component.

In regards to the W501FC gas turbine, the cooling passage of the 1st stage nozzle consists of three separate channels or cavities. Cooling air is supplied from the compressor discharge to either the inlet of each channel or the region between the outer diameter of the nozzles and the inner casing.

The geometry and dimensions of each internal passage was obtained by a direct measurement from a sample nozzle. A detailed description of each channel is discussed in the following:

- The first or leading channel is a straight chamber that contains a single insert divided into two compartments. The first compartment supplies cooling air to the 138 "shower heads" which are arrayed down the leading edge of the vane and orientated toward the pressure-side surface. The second compartment and the internal wall of the cooling passage form an impingement chamber, which has 242 exit holes on the surface of the suction-side surface. No exit holes exist at the inner diameter of the main passage.
- The second or middle channel is a straight chamber that contains a one-compartment insert. This compartment, together with the internal wall of the cooling passage, forms an impingement chamber having 159 surface film-cooling holes on the pressure-side surface. No exit holes are present on the inner diameter of the main passage.
- The third or trailing channel primarily consists of a straight chamber containing a one-compartment insert, an impingement chamber at the outer flange and a chamber at the inner flange. The insert, together with the internal wall of cooling passage, forms another impingement chamber, and its outlet provides cooling flow to a series of pin fins. In addition to a large exhaust slot located at the inner diameter of the main passage, the third channel has a total of 255 holes: (1) 52 on the outer flange for film cooling, (2) 107 on the pressure surface of vane section for film cooling, (3) 30 on the trailing edge of vane section for pin-fin cooling, (4) 38 on the inner flange for film cooling, and (5) 28 exit holes at the bottom of the channel.

A single CPF run was performed for each channel in order to support the complete steady state solution of the nozzle. The inlet pressure and temperature at the cooling flow were estimated to be 224 psia (1.544 MPa) and 680^{o} F (360 ^{o} C). The exit static pressure of main and/or branched passages was estimated based on either the throughflow or external flow solution.

The computed cooling flow at a steady state condition for each of the three channels is listed in **Table 2-3.** It was calculated to be 0.807 lbm/sec (0.154 kg/sec), 0.340 lbm/sec (0.154 kg/sec), and 1.332 lbm/sec (0.604 kg/sec), respectively. The overall cooling flow supplied to 32 nozzles of the first stage becomes 79.3 lbm/sec (36.0 kg/sec), which is about 8.8% of the estimated turbine exhaust flow used in the throughflow analysis, namely, 898 lbm/sec (407 kg/sec).

The calculated gas temperature and film coefficient at the mean-diameter branched passages of the first channel are plotted in **Figure 2-3**. As shown, both film coefficients and gas temperatures increase from the inlet to outlet. The air from main passage directly cools the pressure-side branches while the chamber supplies the cooling air on suction-side branches after the occurrence of impingement cooling. Consequently, the average temperature of 720°F (382°C) on the pressure-side branches is substantially less than the 1030°F (554°C) calculated on the suction-side branches. The averaged film coefficient of 0.00159 Btu/in-in-sec-°F on the pressure-side branches is less than their counterpart on the suction surface of 0.00174 Btu/in-in-sec-°F. This is believed to be mainly due to reduced cooling flow resulting from a larger outlet pressure. The temperature and film coefficient at the chamber was found to be 1014°F (545°C) and 0.00115 Btu/in-in-sec-°F, respectively.

Table 2-3
Steady-State Cooling Flow Distribution

First or Leading Channel	
Pressure Side Surface (138 Exit Holes)	0.262 lbm/sec (0.119 kg/sec)
Suction Side Surface (242 Exit Holes)	0.545 lbm/sec (0.247 kg/sec)
Total Flow (380 Exit Holes)	*0.807 lbm/sec (0.366 kg/sec)*
Second or Middle Channel	
Pressure Side Surface (159 Exit Holes)	0.340 lbm/sec (0.154 kg/sec)
Third or Trailing Channel	
Outer Flange (52 Exit Holes)	0.144 lbm/sec (0.065 kg/sec)
Pressure Side Rows Surface (107 Exit Holes)	0.218 lbm/sec (0.099 kg/sec)
Trailing Edge Pin-Fins (30 Exit Holes)	0.171 lbm/sec (0.078 kg/sec)
Inner Flange (38 Exit Holes)	0.073 lbm/sec (0.033 kg/sec)
Exhaust Slot and 28 Exit Holes	0.726 lbm/sec (0.329 kg/sec)
Total Flow (255 Exit Holes and Exhaust Slot)	*1.332 lbm/sec (0.604 kg/sec)*

The calculated gas temperature and film coefficient at the mean-diameter branched passages of the second channel are shown in **Figure 2-4**. Both film coefficient and gas temperatures increase from inlet to outlet. Because of the impingement cooling that occurs at the chamber between the insert and internal cooling wall, the averaged gas temperature, 1045°F (563°C), is substantially greater than inlet temperature of 680°F (360°C). The mean value of film coefficient is 0.00165 Btu/in-in-sec-°F. In addition, the temperature and film coefficient at the chamber was found to be 1029°F (554°C) and 0.00070 Btu/in-in-sec-°F, respectively.

Table 2-4 lists the averaged gas temperature and film coefficient of each region cooled by the third channel as predicted by CPF. If the region had multiple branches, only the most common value is represented. The results show how the gas temperature at the inner flange is higher than at the outer flange components, principally because heat up occurs along the main cooling passage. The impingement chamber at the airfoil section, formed by the insert and internal wall of main passage, raises the gas temperature to 1054°F (568°C). This thermally elevated cooling flow enters into the pressure-side and pin-fin branched passages. Because the flow rate, geometric configuration and heat transfer mechanism are different in each compartment, the corresponding film coefficient can vary substantially.

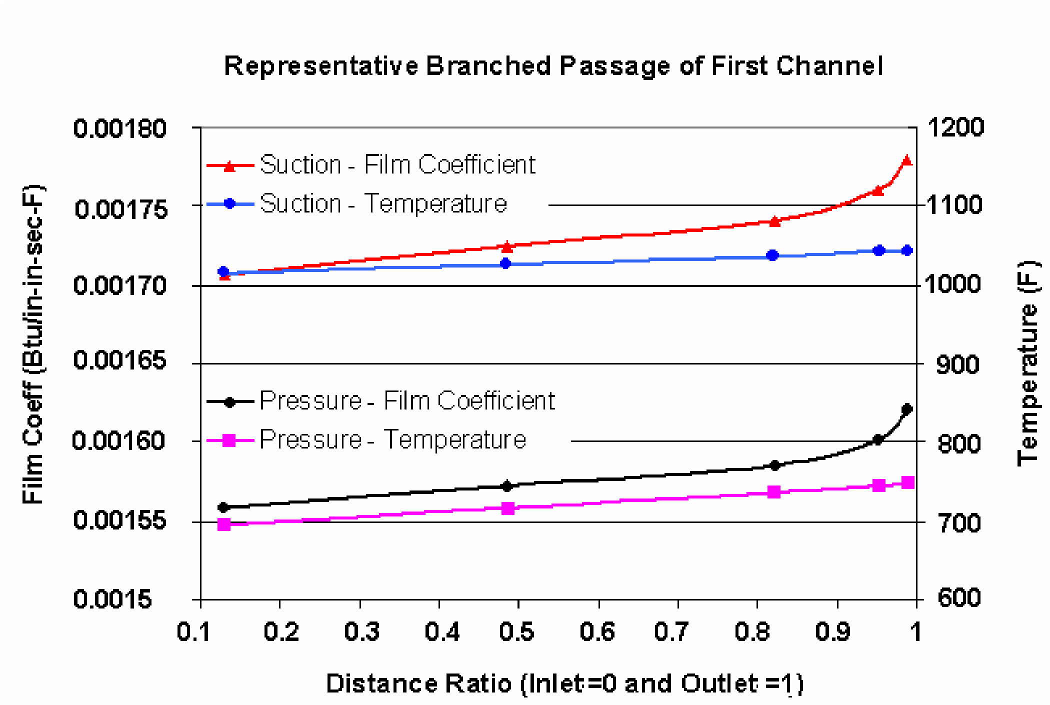

Figure 2-3
Cooling Flow at Mean-Diameter Branched Passages of First Channel

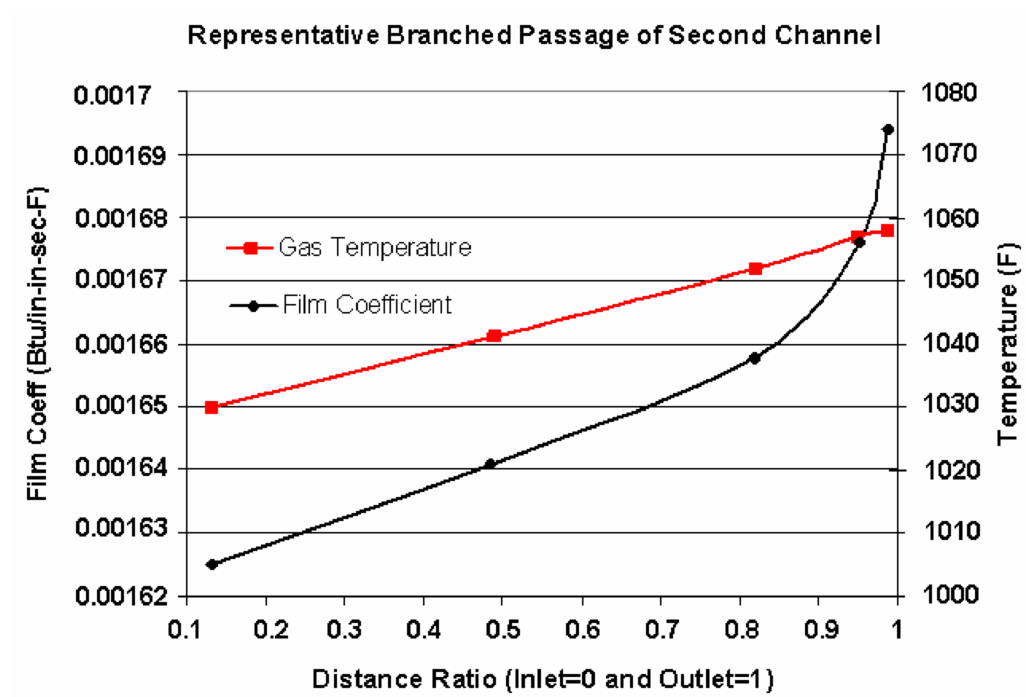

Figure 2-4
Cooling Flow at Mean-Diameter Branched Passages of Second Channel

Table 2-4
Averaged Temperature and Film Coefficients of Third Channel

	Temperature	Film Coefficient
Outer Flange (1) Impingement Shroud	804 ^{o}F (429 ^{o}C)	0.00192 Btu/in-in-sec-^{o}F
(2) Trailing Edge (20 Holes)	957 ^{o}F (514 ^{o}C)	0.00111 Btu/in-in-sec-^{o}F
(3) Pressure Side (32 Holes)	835 ^{o}F (446 ^{o}C)	0.00172 Btu/in-in-sec-^{o}F
Airfoil Section (1) Impingement Chamber	1054 ^{o}F (568 ^{o}C)	0.00106 Btu/in-in-sec-^{o}F
(2) Pressure Side (107 Holes)	1075 ^{o}F (579 ^{o}C)	0.00160 Btu/in-in-sec-^{o}F
(3) Pin Fins (30 Holes)	1162 ^{o}F (628 ^{o}C)	0.00111 Btu/in-in-sec-^{o}F
Inner Flange (1) Impingement Chamber	877 ^{o}F (469 ^{o}C)	0.00070 Btu/in-in-sec-^{o}F
(2) Trailing Edge (22 Holes)	977 ^{o}F (525 ^{o}C)	0.00126 Btu/in-in-sec-^{o}F
(3) Pressure Side (16 Holes)	967 ^{o}F (519 ^{o}C)	0.00135 Btu/in-in-sec-^{o}F

2.3 External Flow Analysis

As discussed at the start of this chapter, the results of the throughflow analysis provided global boundary conditions for each of the stages comprising the turbine, including the first stage nozzles. For the purpose of analyzing the behavior of the individual nozzle a refined CFD analysis of the external gas flow as a boundary layer around the airfoil section is performed based on the parameters defined for the overall environment. An accurate prediction of the convective heat transfer distribution around high-pressure gas turbine blades/nozzles remains an important technical challenge in terms of obtaining a reasonable temperature and stress solution. Besides selecting a suitable turbulence model, the problem is further complicated by the fact that a non-negligible portion of the boundary layer developing around these surfaces is in a transitional state. A number of research papers have been published to not only predict the correct behavior of the onset of transition, but also estimate the length between the laminar and turbulent layers. Different transition models can lead to substantially different distributions of film coefficients along the airfoil profile. The applied CFD program must therefore be sufficiently sophisticated to solve the complex boundary layer problem.

In developing the HSLMP, the quasi-3D rotor viscous program developed by NASA, RVCQ3D [6] was originally selected and adapted to carry out the external flow analysis for airfoil sections.

Developed and verified for aircraft turbine applications, the code solves the thin-layer Navier-Stokes equation on a blade-to-blade revolution using an explicit finite-difference technique. By incorporating various transition models defined by transition length and transition intermittency, a modified version of the RVCQ3D program [6] was able to validate and compare the film coefficients predicted from tests of different theories. This modified RVCQ3D program is presently considered to represent the most up-to-date technology for dealing with the boundary layer problem in regards to turbomachinery cascade applications.

An extensive effort was made to choose the 'right' transition model used in the present investigation. An extensive literature survey and technical discussions with NASA led to the selection of appropriate models to (1) predict the start of transition, (2) evaluate the transition length, (3) estimate the transition intermittency, and (4) govern the turbulence after transition. A number of features such as the relaminization issue, the influence due to free stream and/or upstream turbulence, and Mach number effects were employed to configure the transition model.

The two-dimensional CFD mesh actually used to simulate the flow path at mean section is shown in **Figure 2-5**. It is a C-shaped grid with a mesh size of 60 x 338 elements. The grid spacing away from the airfoil space is extremely small, i.e. less than 2.0×10^{-4} inch (5×10^{-3} mm), which is a prerequisite to achieve an accurate evaluation of film coefficients.

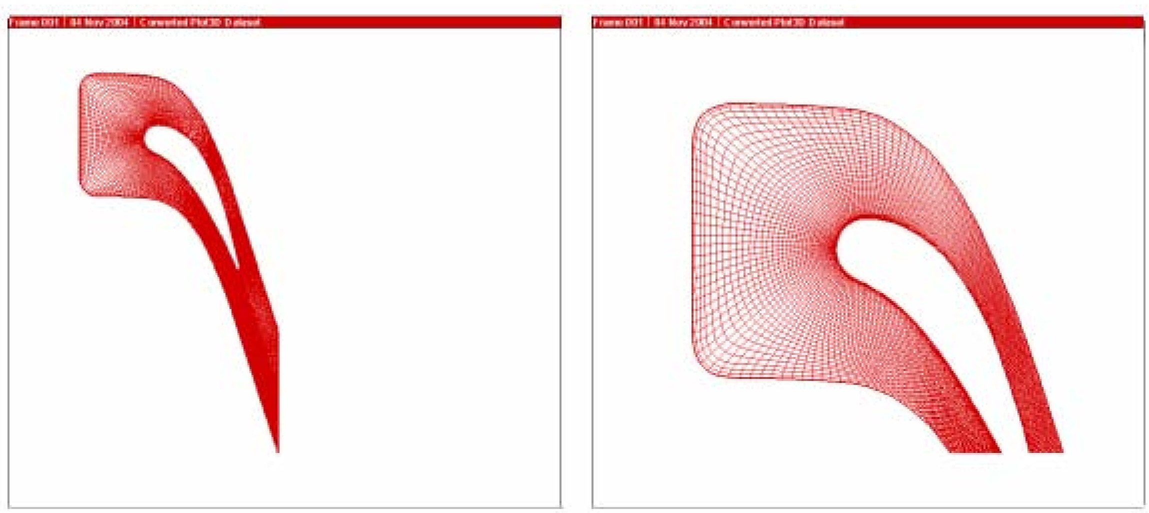

Figure 2-5
CFD Mesh at Flow Path of Mean Section

In a typical RVCQ3D run, the inlet boundary conditions of total temperature, total pressure, and flow angle, and the exit boundary condition of static pressure are specified. The flow under consideration is compressible and turbulent, with an inlet turbulence intensity of 0.08 and an inlet turbulence length scale of 0.0001. The conservation of energy equation is solved to give the total temperature throughout the flow domain. Air properties were used for the thermal conductivity, specific heat and viscosity of the gas, which are calculated as a function of the local temperature. By specifying temperature distribution on the airfoil surfaces, the code was then able to compute the heat flux across the surface of the nozzle using the equation:

$$q = -k_f \left. \frac{\partial T}{\partial n} \right|_{n=0}$$

where k_f is the thermal conductivity of the gas and $\left. \frac{\partial T}{\partial n} \right|_{n=0}$ is the temperature gradient in the direction normal to the surface, measured at the wall. The modified RVCQ3D program further calculates the film coefficient, h, at each cell, for the given surface temperature, T_s, and a specified bulk flow temperature, T_b as:

$$h = \frac{q}{(T_s - T_b)}$$

Under steady state operations the static pressure and Mach number distribution at mean diameter location are shown in **Figure 2-6**. The static pressure (on the left) has a unit of 'psia'. As would be expected, the largest pressure of 214 psia (1.475 MPa) is present at the leading edge of the pressure-side profile. The smallest pressure, 148 psia (1.020 MPa), occurred near mid-span of the suction-side profile. The Mach number distribution is essentially opposite to the static pressure distribution. Namely, the larger the static pressure, the smaller the Mach number. The maximum number of 0.728 indicates the flow field is subsonic. A distinctive wake region, featuring a lower Mach number after the trailing edge could be observed as well.

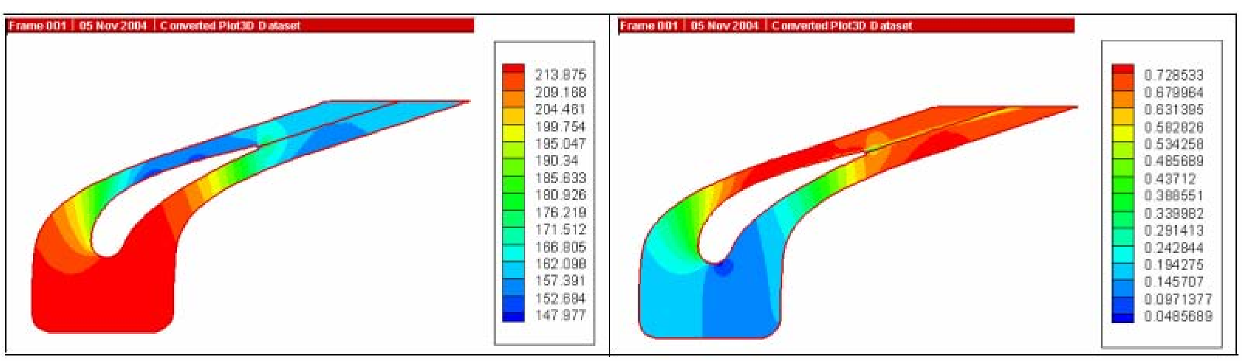

Figure 2-6
Static Pressure and Mach Number Distribution

Figure 2-7 shows the variation of film coefficients evaluated at the mean diameter under steady state operation, where the leading edge denotes a reference for distance. The stagnation point is located at the pressure side, approximately 0.30 inch (7.6 mm) away from the leading edge. The film coefficient at the stagnation point is about 0.00068 Btu/in-in-sec-°F. The maximum heat transfer rate at the suction side surface, 0.00086 Btu/in-in-sec-°F, occurs at the region about 2.5-

3.5 inches away from the stagnation point. The maximum heat transfer rate at the pressure side surface was found to be 0.00078 Btu/in-in-sec-°F, occurring near the trailing edge.

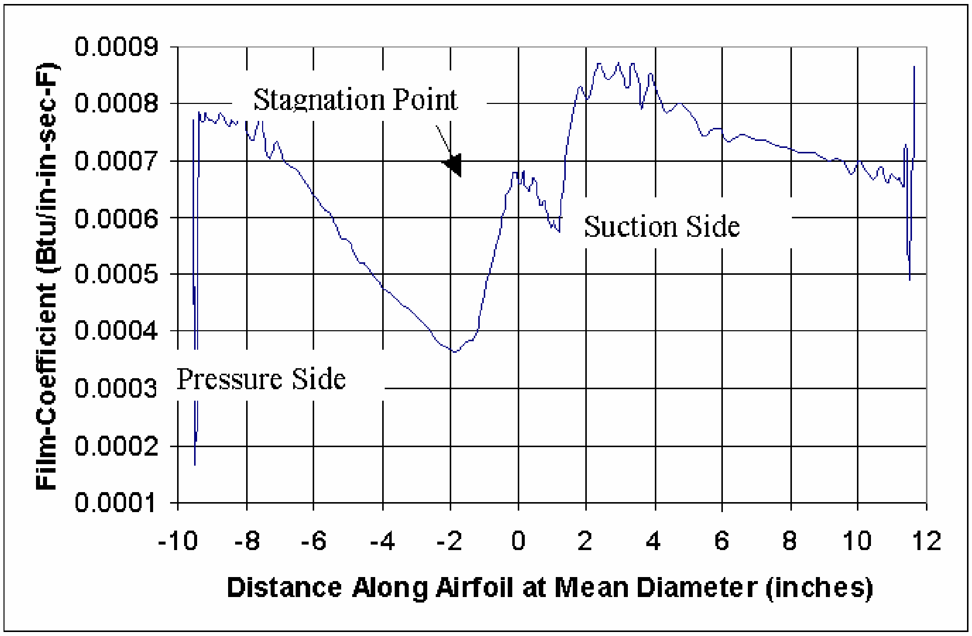

Figure 2-7
Variation of Film Coefficient Predicted at Mean Diameter

On the pressure side surface, the transition shows up at 2 inches (51 mm) from leading edge. Relaminization of boundary layer flow probably has a profound effect to raise the film coefficient from 0.00037 Btu/in-in-sec-°F at transition to 0.00078 Btu/in-in-sec-°F near the trailing edge. The recovery of heat transfer rate is most significant in the first 5.0 inches (127 mm) away from the transition point. On the suction side surface, the transition appears at about 1.2 inches (30 mm) from the leading edge, with a film coefficient of 0.00058 Btu/in-in-sec-°F. The heat transfer rate quickly recovers in a short distance. It reaches the maximum value of 0.00086 Btu/in-in-sec-°F within a short distance, and then decreases gradually until it approaches the trailing edge.

Note that as a result of severe disturbance at the wake region, a substantial variation of film coefficient is present near the trailing edge.

3
VERIFICATION OF INTERNAL COOLING

To successfully determine the steady state response of W501 FC 1st stage nozzles, accuracy in the distribution of heat transfer coefficients and temperatures within the cooling passages are essential. Like building a house, the throughflow defines the boundaries of the lot or chosen site. The internal cooling analysis is the foundation on which the strength of the subsequent floors ultimately depends. The CPF program involves certain idealizations and assumptions to deal with the complicated geometry such as the insert within each cavity, shower head and film cooling holes at the first cavity, film cooling holes of the second cavity, outer shroud and inner shroud chamber, film cooling holes, and pin-fins at the third cavity. Since direct verification of these analytical results was not possible due to a lack of any published data on operating W501 FC 1st stage nozzles, verification of the CPF analysis was pursued by independently testing the flow. This test was conducted on a complete nozzle substituting air for gas and comparing the results against those predicted by CPF.

3.1 Test Design

The primary objective of the test was to obtain experimental data for an actual W501 FC gas turbine first stage nozzle, which in turn could be used establish the mass flow of air exiting each surface cooling hole and transition hole. This was to be obtained at a variety of deferential pressures to further check the consistency between results. Earlier programs to measure air exiting cooling orifices on 9FA and 7FA+1st row buckets had demonstrated the inherent variability that could be introduced due to (a) the probe and technique by which it was supplied, (b) the quality and stability of the air supplied to the component, and (c) issues related to instrument sensitivity and calibration. The nozzle test was therefore designed to address these issues and also streamline the data collection process, as it ultimately required data at three pressure points on each of the 794 individual cooling orifices listed in **Table 1-1**.

As shown in **Figure 3-1**, the test set up involved a large capacity portable “instrument air” quality compressor, connected to a precision mass flow sensor (Coriolis effect type), followed by a large capacity regulator. This insured that all air eventually delivered to the test nozzle was (a) cooled to ambient temperature, (b) filtered and (c) accurately measured in pounds per minute. The exit air probe was also carefully designed with custom tips to minimize backpressure and allow consistent sealing of the probe to the surface as each orifice was isolated and sampled. Experience had shown that poor probe contact may introduce a venturi effect and exaggerate the flow rate. All probe flow was directed through a gas flow sensor (hot wire type). Having a known and accurate input flow value allowed a consistent correction factor to be applied to the readings based on a comparison of the combined orifice flow rates to the known input value.

Figure 3-1
Compressor and Regular Used in Airflow Test

3.2 Test Methodology

In each series of tests the compressor air was allowed to stabilize at ambient temperature. The conditioned air was supplied to the mass flow sensor at approximately 100 psig. The pressure regulator was manually adjusted to provide the desired test pressure reading from the pressure transducer located on the manifold connection flange at the nozzle input. Test data points were taken at 10, 30 and 50 psig. Adjustments were made as necessary to maintain the pressure point within ±0.2 psi. Pressure readings were manually entered in the data collection spreadsheet for a given group of orifices being probed. The input mass flow rate was read and also manually entered in the spreadsheet.

A frame of heavy aluminum bar stock was machined and fitted to the input end of the nozzle, serving as a structural base for the first and second cavity manifolds and as the chamber for the third cavity. All joints were sealed with an RTV. As previously described, the 501 FC nozzles contain three identifiable flow sections, whereby each section supplies specific groups of cooling holes on the nozzle surface. To isolate each section, or "cavity" for testing, a custom manifold was designed. **Figure 3-2** shows the manifold for the third cavity. **Figure 3-3** shows the manifold for the first cavity.

To test any single cavity, the remaining two were capped to isolate them from the supply air. In **Figure 3-2**, the picture on the left shows how the first cavity is capped and the cap of the second about to be installed.

Figure 3-2
Third Cavity Manifold

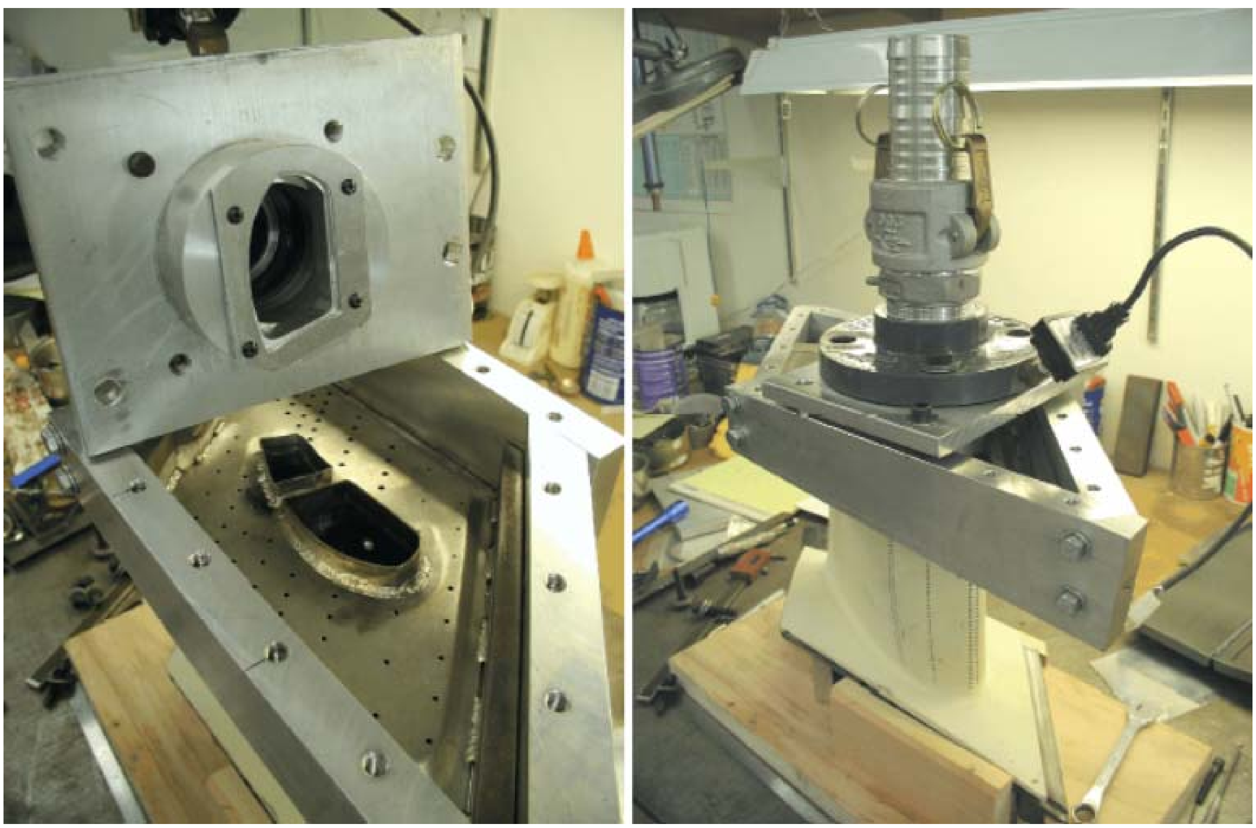

Figure 3-3
First Cavity Manifold

Standard air gun tips mere modified to allow optimum placement and sealing for the different sizes and types of holes. The probe tips, mass flow sensor and probe assembly are shown in **Figure 3-4**. The ID of the tip holes were sized to be larger than the holes being measured and the tip shape ground to suit the typical surface. A prerequisite of the tips were that they could not be allowed to influence the adjacent orifices by obstructing them. The trailing edge holes required a special shape to accommodate their being slightly recessed. From the rubber tip and beyond to the flow sensor, the ID of the flow path increased rapidly to minimize backpressure.

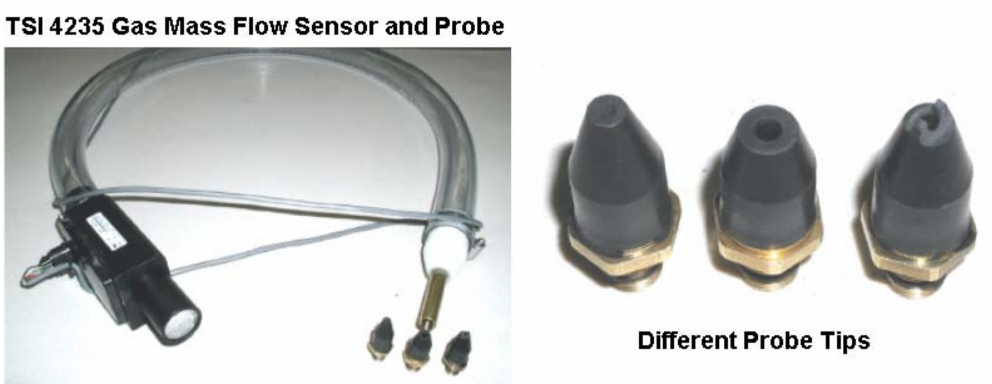

Figure 3-4
Probe Tips and Assembly of Mass Flow Sensor & Probe

The probe and an example of raw data for each of the five arrays down the lead edge are shown in **Figure 3-5**. Typical data collection for a given supply pressure started with pressing the probe tip over an orifice and watching the meter display for signal stability. Slight position shifting was used to seek a maximum reading, indicating that the tip was not partially blocking the test orifice. When the reading appeared optimized, a foot switch was used to send the data from the meter to a laptop spreadsheet via RS232 and Win Wedge communications software. All holes were mapped and organized to match a spreadsheet template for ease of data collection.

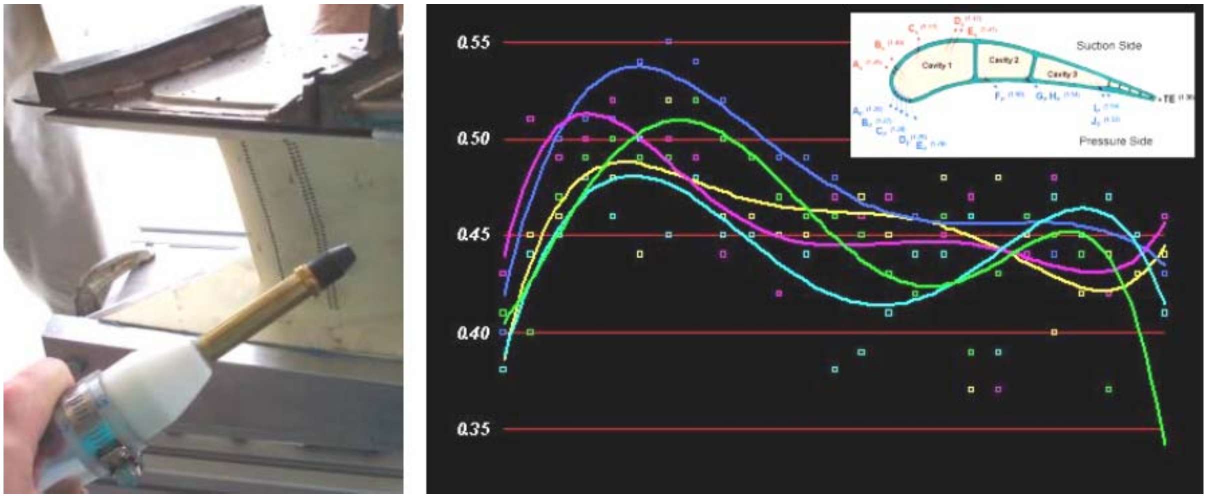

Figure 3-5
Probe on Cooling Orifice and Data

3.3 Exit Hole Mapping

Flow data was taken for all orifices (or exit holes) on the nozzle at a consistent pressure to minimize adjustments to the regulator control. Supply pressure and input mass flow were observed and manually entered into each orifice data group. Exit flow readings were taken sequentially on each row or group, starting with the orifices closest to the supply, numbered one through the last for each group. The raw data spreadsheet was presented electronically. The exit holes were grouped and numbered as shown in **Figure 3-6** and **Figure 3-7**.

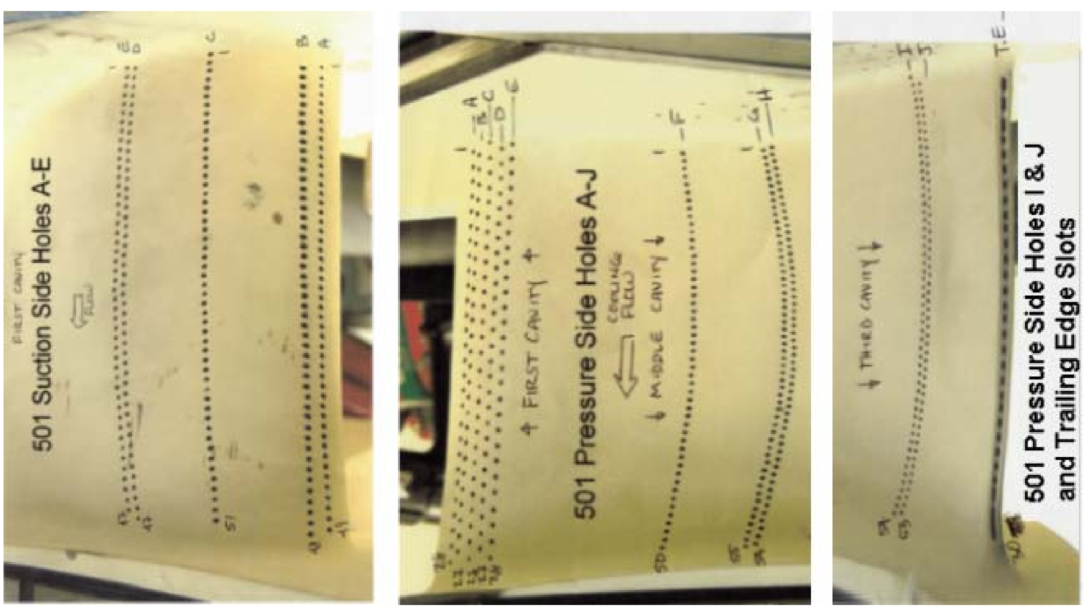

Figure 3-6
Referenced Exit Holes on Suction and Pressure Side of Airfoil

Figure 3-7
Numbering of Exit Holes at Outer and Inner Flange of Third Cavity

3.4 Summary of Flow Measurements

All orifice flow readings were totaled by groups and finally by cavity identification. These are summarized in **Table 3-1** for each of the supply pressures of 10, 30 and 50 psig. The unit expressed for mass flow rate is lbm/min. In general it was observed that cavity #3 would accommodate the maximum airflow, while cavity #2 would allow the minimum airflow under the same supply pressure.

Table 3-1
Summary of Measured Air Flow at Various Supply Pressures

Cavity #1			
	Supply Pressure 10 psig	Supply Pressure 30 psig	Supply Pressure 50 psig
Pressure Side Rows A-E (138 Exit Holes)	5.39	9.99	14.60
Suction Side Rows A-E (242 Exit Holes)	8.54	16.21	23.04
Total Flow (380 Exit Holes)	*13.93*	*26.20*	*37.64*
Cavity #2			
	Supply Pressure 10 psig	Supply Pressure 30 psig	Supply Pressure 50 psig
Pressure Side Rows F-H (159 Exit Holes)	5.95	9.80	13.40

Table 3-2
Summary of Measured Air Flow at Various Supply Pressures (Continued)

Cavity #3			
	Supply Pressure 10 psig	Supply Pressure 30 psig	Supply Pressure 50 psig
Outer Flange Trailing Edge (20 Exit Holes)	1.257	2.464	3.582
Outer Flange Pressure Side (32 Exit Holes)	0.822	1.580	2.294
Pressure Side Rows I-J (107 Exit Holes)	2.147	3.793	5.540
Trailing Edge Pin-Fins (30 Exit Holes)	1.874	4.530	6.587
Inner Flange Trailing Edge (22 Exit Holes)	0.264	0.489	0.678
Inner Flange Pres. and Suc. Side (16 Exit Holes)	0.553	0.997	1.406
Adders and 28 Exit Holes (A1-A8, B1-B15, C1-C5)	6.583	12.847	19.313
Total Flow (255 Exit Holes)	*13.500*	*26.700*	*39.400*

3-5 Correlation of CPF Results with Air Flow Results

The mass flow rates of the first cavity measured by the airflow tests and computed by the CPF program are presented in **Table 3-2** for a supply pressure of 10, 30 and 50 psig. As shown, the results for the first cavity are in excellent agreement, with no more than a 2.2% difference between the summation of mass flow for both pressure side and suction side exit holes.

Table 3-3
Air Flow Comparison of First Cavity

Supply Pressure=10 psig			
	Test (lbm/min)	CPF (lbm/min)	Difference (%)
Pressure Side Rows A-E (138 Exit Holes)	5.39	5.33	-1.1
Suction Side Rows A-E (242 Exit Holes)	8.54	8.35	-2.2
Total Flow (380 Exit Holes)	13.93	13.68	-1.8
Supply Pressure=30 psig			
	Test (lbm/min)	CPF (lbm/min)	Difference (%)
Pressure Side Rows A-E (138 Exit Holes)	9.99	9.94	-0.5
Suction Side Rows A-E (242 Exit Holes)	16.21	15.90	-1.9
Total Flow (380 Exit Holes)	26.20	25.84	-1.4
Supply Pressure=50 psig			
	Test (lbm/min)	CPF (lbm/min)	Difference (%)
Pressure Side Rows A-E (138 Exit Holes)	14.60	14.50	-0.7
Suction Side Rows A-E (242 Exit Holes)	23.04	22.88	-0.7
Total Flow (380 Exit Holes)	37.64	37.38	-0.7

The mass flow rate comparison of the second cavity is given in **Table 3-3**. A reasonably good agreement was still observed by examining the measured and calculated results, although not of the outstanding quality as in the first cavity. At a supply pressure of 10 psig, the CPF results were 7.9% lower than the measured data. In contrast, the CPF results were higher than the measured data for the other two supply pressures.

Table 3-4
Air Flow Comparison of Second Cavity

Supply Pressure=10 psig			
	Test (lbm/min)	CPF (lbm/min)	Difference (%)
Pressure Side Rows F-H (159 Exit Holes)	5.95	5.48	-7.9
Supply Pressure=30 psig			
	Test (lbm/min)	CPF (lbm/min)	Difference (%)
Pressure Side Rows F-H (159 Exit Holes)	9.80	10.29	+5.0
Supply Pressure=50 psig			
	Test (lbm/min)	CPF (lbm/min)	Difference (%)
Pressure Side Rows F-H (159 Exit Holes)	13.40	14.77	+10.2

As shown in **Table 3-4**, the mass flow rate of the third cavity was the most complicated, and required that it be divided into seven groups to provide additional comparisons. Although the following individual discrepancies were noted, the overall mass flow predicted by CPF still agreed very well with the test data, with the largest difference of 7.0% was with the data taken at the supply pressure of 50 psig. As to the behavior of regions within the third cavity:

<u>In the outer flange</u> the mass flow at trailing edge holes had a discrepancy, 19.0%, 16.4%, and 18.1% at the supply pressure of 10, 30, and 50 psig, respectively. The difference in mass flow taken from the pressure side holes is held to no more than 6.8%. The maximum difference of 29.4% occurred from measurements of rows I-J on the pressure side of airfoil, at a supply pressure of 30 psig. This group of holes also showed a substantial variation with respect to the supply pressure of 10 psig and 50 psig. The mass flow at the trailing edge associated with pin fins shows a slight variation in the range between 0.9% and 8.3%.

<u>In the inner flange</u> the difference of mass flow at trailing edge varies substantially: 3% for a supply pressure of 10 psig and 23.4% for a supply pressure of 50 psig. The difference of mass flow between the pressure/suction side holes is less than 10.7%. The mass flow difference at the cavity exhaust corresponding to the supply pressure of 10, 30, and 50 psig was found to be 6.9%, 16.6%, and 10.1%, respectively.

Table 3-5
Air Flow Comparison of Third Cavity

Supply Pressure=10 psig			
	Test (lbm/min)	CPF (lbm/min)	Difference (%)
Outer Flange Trailing Edge (20 Exit Holes)	1.257	1.018	-19.0
Outer Flange Pressure Side (32 Exit Holes)	0.822	0.786	-4.4
Pressure Side Rows I-J (107 Exit Holes)	2.147	2.448	+14.0
Trailing Edge Pin-Fins (30 Exit Holes)	1.874	2.029	+8.3
Inner Flange Trailing Edge (22 Exit Holes)	0.264	0.272	+3.0
Inner Flange Pressure and Suction Side (16 Exit Holes)	0.553	0.494	-10.7
Adders and 28 Exit Holes (A1-A8, B1-B15, C1-C5)	6.583	7.039	+6.9
Total Flow (255 Exit Holes)	13.500	14.086	+4.3
Supply Pressure=30 psig			
	Test (lbm/min)	CPF (lbm/min)	Difference (%)
Outer Flange Trailing Edge (20 Exit Holes)	2.464	2.058	-16.4
Outer Flange Pressure Side (32 Exit Holes)	1.580	1.515	-4.1
Pressure Side Rows I-J (107 Exit Holes)	3.793	4.911	+29.4
Trailing Edge Pin-Fins (30 Exit Holes)	4.530	4.433	-2.1
Inner Flange Trailing Edge (22 Exit Holes)	0.489	0.568	+16.1
Inner Flange Pressure and Suction Side (16 Holes)	0.997	1.019	+2.2
Adders and 28 Exit Holes (A1-A8, B1-B15, C1-C5)	12.847	14.985	+16.6
Total Flow (255 Exit Holes)	26.700	28.489	+6.7
Supply Pressure=50 psig			
	Test (lbm/min)	CPF (lbm/min)	Difference (%)
Outer Flange Trailing Edge (20 Exit Holes)	3.582	2.933	-18.1
Outer Flange Pressure Side (32 Exit Holes)	2.294	2.137	-6.8
Pressure Side Rows I-J (107 Exit Holes)	5.540	6.972	+25.8
Trailing Edge Pin-Fins (30 Exit Holes)	6.587	6.530	-0.9
Inner Flange Trailing Edge (22 Exit Holes)	0.678	0.837	+23.4
Inner Flange Pressure and Suction Side (16 Holes)	1.406	1.498	+6.5
Adders and 28 Exit Holes (A1-A8, B1-B15, C1-C5)	19.313	21.265	+10.1
Total Flow (255 Exit Holes)	39.400	42.172	+7.0

3.6 Summary of Test Results

After a close examination of the measured and computed mass flow rate for each of the three supply pressures which were tested, the following conclusions were drawn:

- The calculated mass flow rates predicted by CPF correlated well with the measured data, considering the uncertainty and variation involved in the test, the idealizations and assumptions incorporated in the numerical analysis and the extremely complicated geometry including 794 exit holes.
- The first cavity had both showerhead and film cooling holes while the second cavity consists of film cooling holes only. This geometric variation is believed to be the reason why the mass flow correlation of the first cavity is superior to that of the second cavity. A number of empirical equations incorporated into CPF allowed, in this instance, for it to simulate the cooling through the array of flow passages more precisely than for the other arrangements. Despite this limitation, the correlation was still quite acceptable for the purpose of calibrating the CPF model of the cavity.
- In addition to film cooling holes and pin fins on the airfoil section, the third cavity contains (a) an impingement chamber at the outer and inner flange, (b) an exhaust and (c) a number of exit holes at the bottom of the passage. Considering the complexity and limitation of numerical implementations within CPF, the difference of the overall flow rate of less than 7%, was acceptable for the purpose of supporting the aero thermal analysis, even though certain sub-group correlations generated a discrepancy of more than 20%. Guided by the test results, CPF was further modified to deal with these specific arrangements, and an iterative algorithm was established to also balance the inlet and outlet mass flow.

To summarize, the test provided extremely valuable insight as to how the complex internal and external geometry of the nozzle utilized and distributed the flow made available to it. The results obtained at different supply pressures proved to be consistent and reproducable. The initial correlation between the measured and predicted results was surprisingly good, particularly for the first cavity. Results for the second and third cavities further provided a basis to make reasonable and appropriate adjustments to the cooling models, based on the camparisons. In general, the verification of the CPF models provided the basis to proceed with the remaining steps of the analysis with a much higher level of confidence than would have been possible without the results of the detailed survey of the flow.

4
THERMAL ANALYSIS

With the internal and external flow analyses completed, the next step in the process of evaluation was to integrate the results with the structural model of the nozzle, and calculate the temperatures that result as an equilibrium between internal cooling and gas flow is achieved. This precedes the calculation of stresses, based on the temperatures produced from this effort.

4.1 Finite Element Model

A 3-D finite element model (**Figure 4-1**) was generated utilizing the commercially available program ANSYS. The model eventually consisted of approximately 100,000 eight-node brick elements. It included almost all of the critical features found in a typical nozzle segment, namely, the airfoil or vane, the outer shroud, the inner shroud and all 767 convective, film cooling and pin-fin cooling holes. The TBC system with a ceramic layer and a bond coat was also included. The thickness of the TBC and NiCoCrAlY bond coat was assumed to be 7 mils (0.178mm). As published material properties for ECY768 (used in the 1st stage nozzle) were not available, properties of the similar cobalt-based alloy Mar-M509 were substituted.

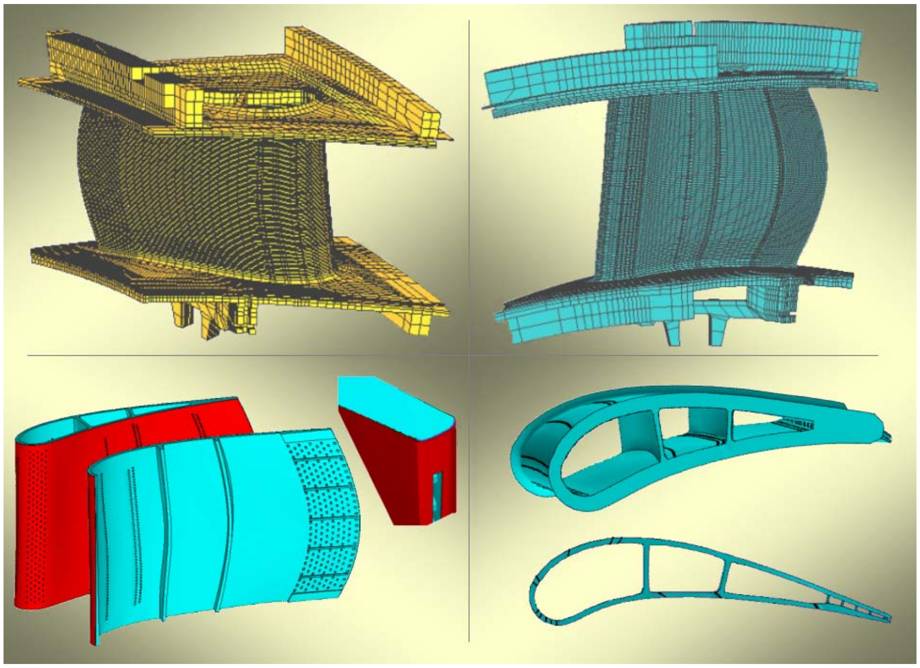

Figure 4-1
Element and Surface Plots of the W501FC 1st Stage Nozzle FE Model

The corresponding physical and elastic properties of Mar-M509 are shown in **Figure 4-2**. Properties of the nickel-based alloy IN738 originally used to evaluate the complementary 1st stage rotating blade are included in the same figure for a comparison. The thermal conductivity and thermal expansion coefficient of Mar-M509 are noticeably higher than IN738. Mar-M509 also has a higher Young's modulus in the low temperature regime. Both materials have superior high temperature resistance against oxidation and corrosion. Mar-M509 is relatively easier to weld in regards to its repair. Also, as a cobalt-based alloy, it is denser than a nickel-based alloy. The density of Mar-M509 is about 0.32 lbm/in^3 compared to 0.293 lbm/in^3 of IN738. Density is an important consideration when designing blades, because centrifugal loads are naturally diminished when the density of the material is reduced.

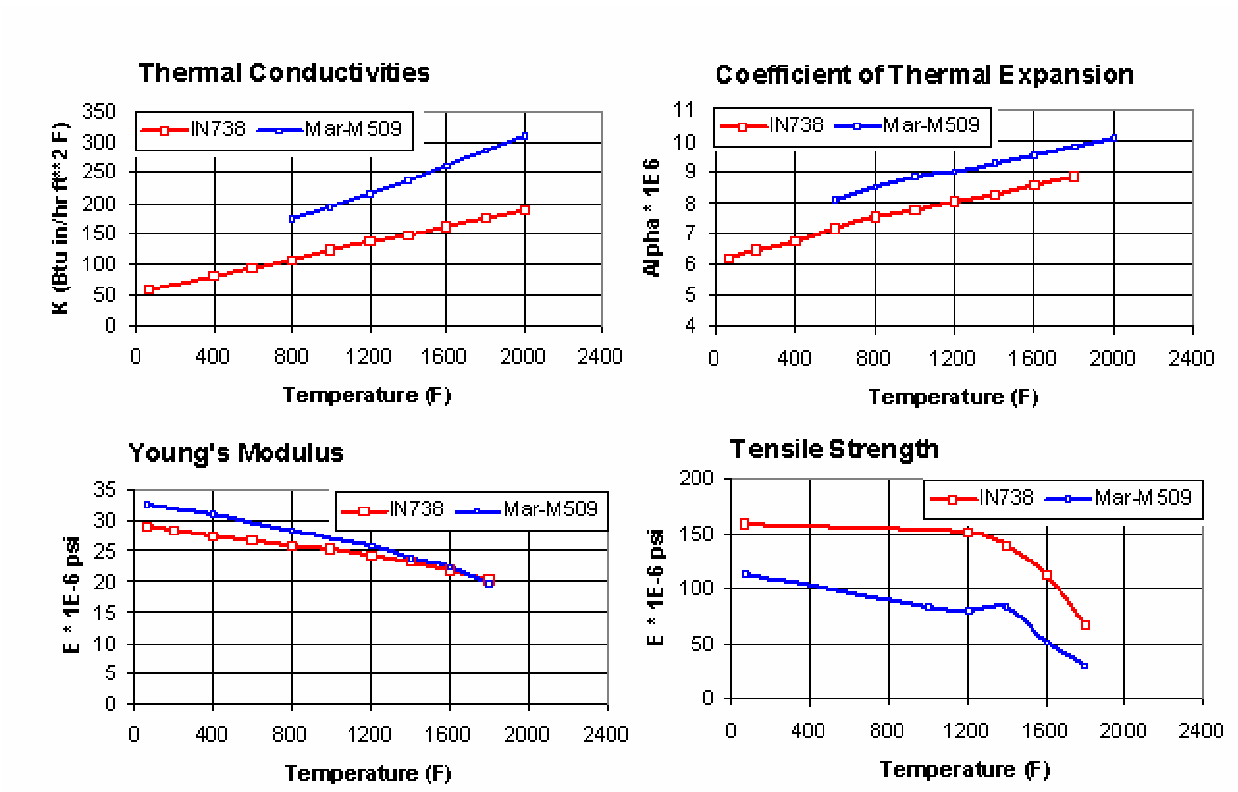

Figure 4-2
Physical and Mechanical Properties of Mar-M509

As stated, the nozzle model was purposely designed to efficiently interface and automatically transfer the boundary conditions resulting from the external heating and internal cooling calculations. Meshing was undertaken in an ordered fashion to effectively achieve this link with the flow models. Temperature dependent material properties were used throughout the analysis.

4.2 Steady State Results

The heat conduction analysis for the W501FC 1st stage nozzle was performed by applying thermal boundary conditions generated from the previously described external and internal heat transfer analyses. A plot of the resulting temperature distribution throughout the nozzle at base load operation is shown in **Figure 4-3**. From these results, a peak temperature of 2066° F (1130° C) was predicted to occur on the surface of the TBC layer, appearing at the vane trailing edge approximate to the inner shroud. The corresponding interface temperature between the TBC and bond coat was calculated to be about 1783°F (973°C).

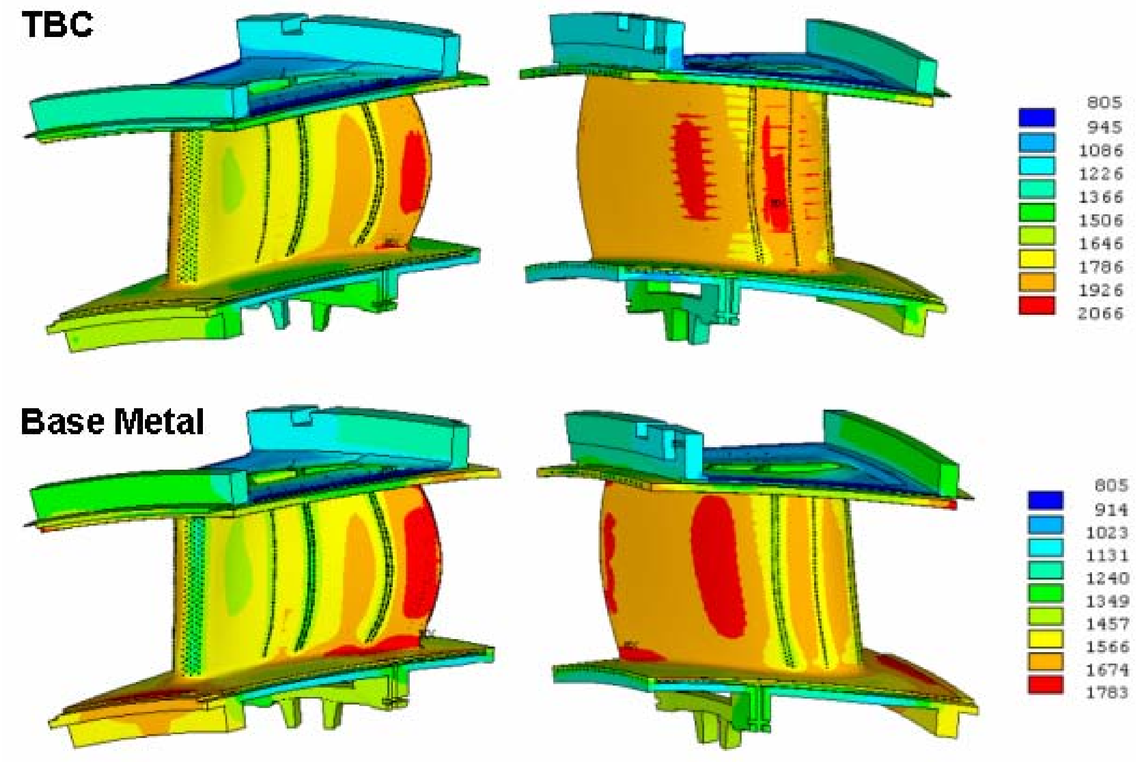

Figure 4-3
Predicted Temperature Distributions for W501FC 1st Stage Vane

Figure 4-4 shows the predicted temperature distribution though the TBC layers at 50% of the vane height. The metal temperature is between 200º F ~ 350º F (111º C ~ 194º C) lower than the temperature in the top (outer) layer as a result of the lower thermal conductivity of the ceramic coating. The effectiveness of local cooling can be measured by cooling effectiveness η as:

$$\boldsymbol{\eta = (T_g - T_m)/ (T_g - T_c)}$$

where T_g is the gas temperature, T_m is surface metal temperature and T_c is the corresponding cooling air temperature. **Figure 4-5** depicts the cooling effectiveness at 50% of the vane height. The overall cooling at this height was predicted to be in the range 60% to 85% effective.

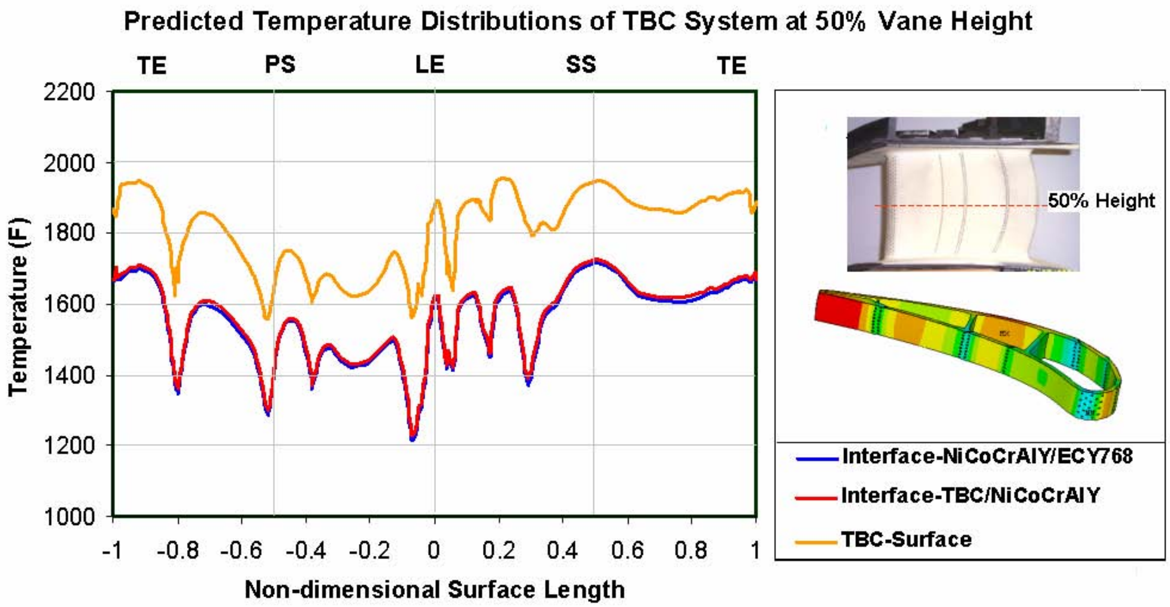

Figure 4-4
Predicted Temperature Distributions of TBC Layers

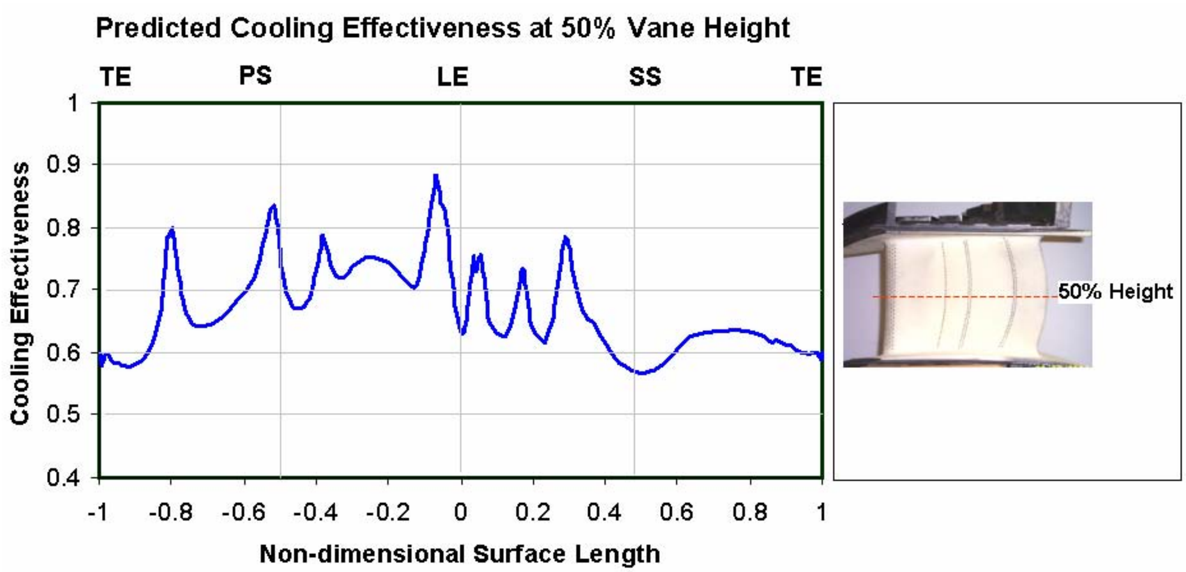

Figure 4-5
Predicted Cooling Effectiveness

It would appear from these results that sufficient cooling is directed to most of the principal region of the airfoil that takes the brunt of the hot gas flow. This is testimony to the advanced cooling configuration and TBC system employed by the 1st stage vane. Higher conductivity of a cobalt-based super alloy would further reduce the temperatures in the base metal. **Figure 4-6** compares temperature distributions in the TBC for Mar-M509 and IN738 base metal materials. The benefit of using a cobalt-based alloy to lower metal temperatures is clearly demonstrated in this figure.

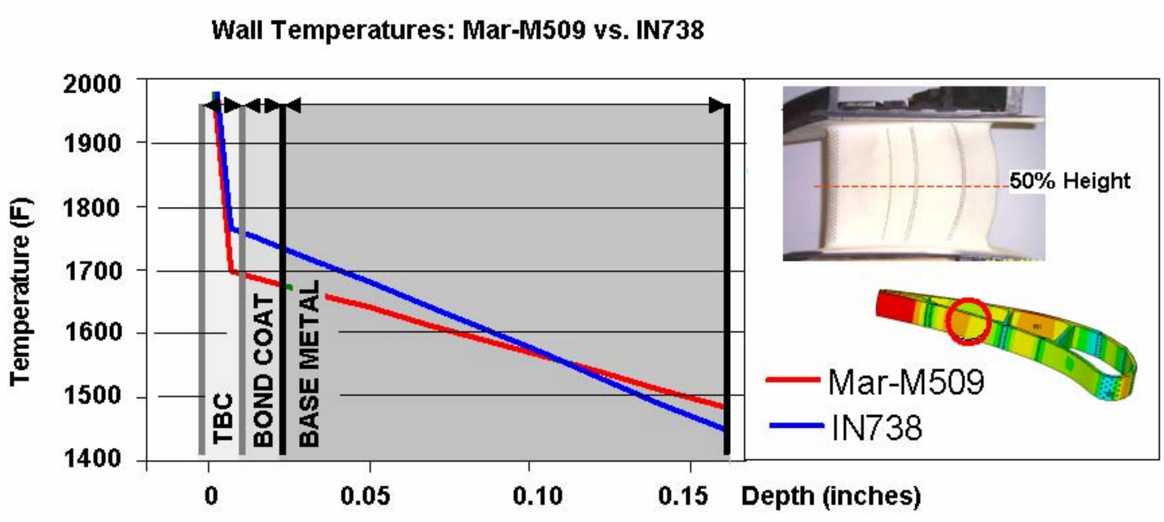

Figure 4-6
Temperature Distribution for TBC Coated Nozzle Using Different Base Metals

The firing temperature of the 501FC design is approximately 400ºF (204°C) higher than that of the 501D design. As a result of advances in cooling techniques, the average metal temperatures of the 501F design are likely to be comparable or even lower than those of the 501D design. Although the overall bulk metal temperature appears to be reasonable in view of the extremely high gas temperature environment localized high temperature gradients are present, particularly in the sidewall fillet and regions of the shroud. From the history of hot section applications it is known that locations with high temperature gradients are very likely to experience high stresses which lead to cracking as a consequence of thermal cycling. **Figure 4-7** shows the predicted temperature distributions along the juncture between the vane and inner shroud.

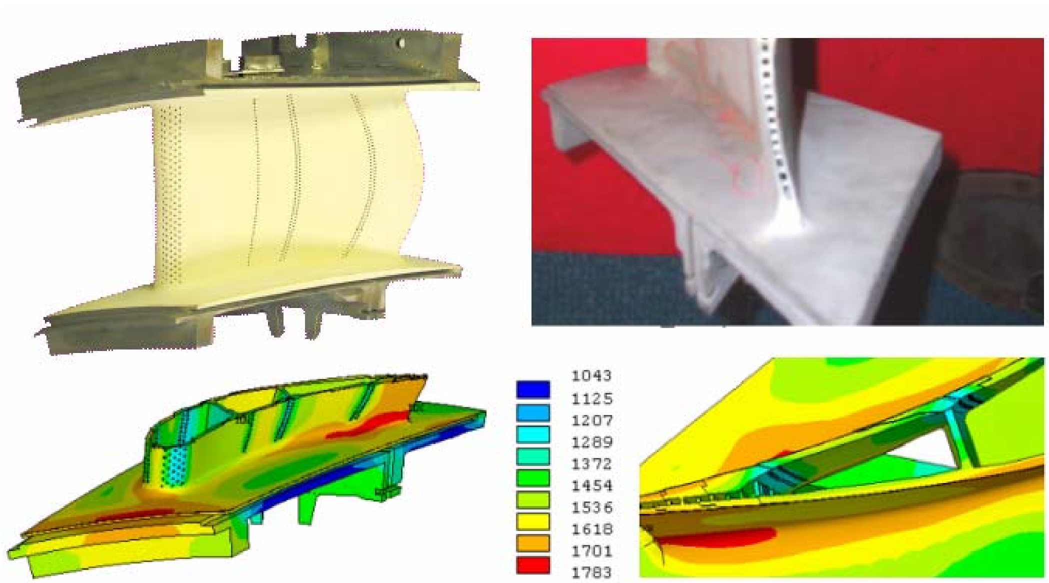

Figure 4-7
Predicted Temperature Distributions near Inner Fillet Region

Considerably high temperatures and temperature gradients were found at the inner fillet on the pressure side, near the hub region of the 3rd cavity. Surface metal temperature at this location was predicted to be around 1700º F (927º C).

From these results it would appear that the primary failure mechanism of critical inner fillet cracking is not likely caused by time-dependent high temperature oxidation. The severe inner fillet cracking is instead suspected to be associated with thermal stress induced from a high temperature gradient during thermal cycling. This was pursued in the next step of the analysis.

5
STRESS ANALYSIS

A structural finite element model in parallel with the heat conduction model was constructed for the calculation of stress. The temperature dependent material properties of Mar-M509, NiCoCrAlY and Y_2O_3-ZrO_2 were used for the base metal, bond coat and TBC, respectively. A stress analysis was performed for the 1^{st} stage vane by applying calculated temperatures as body forces.

5.1 Stress Results

Figure 5-1 shows the equivalent stress distributions throughout the vane and shrouds. The contours are plotted to show the surface of the base metal and surface of the TBC. Overall, stress in the topcoat of the TBC is about 20 ksi lower throughout the vane than in the base metal underneath. A maximum stress of about 25 ksi was calculated on the topcoat in the inner shroud region.

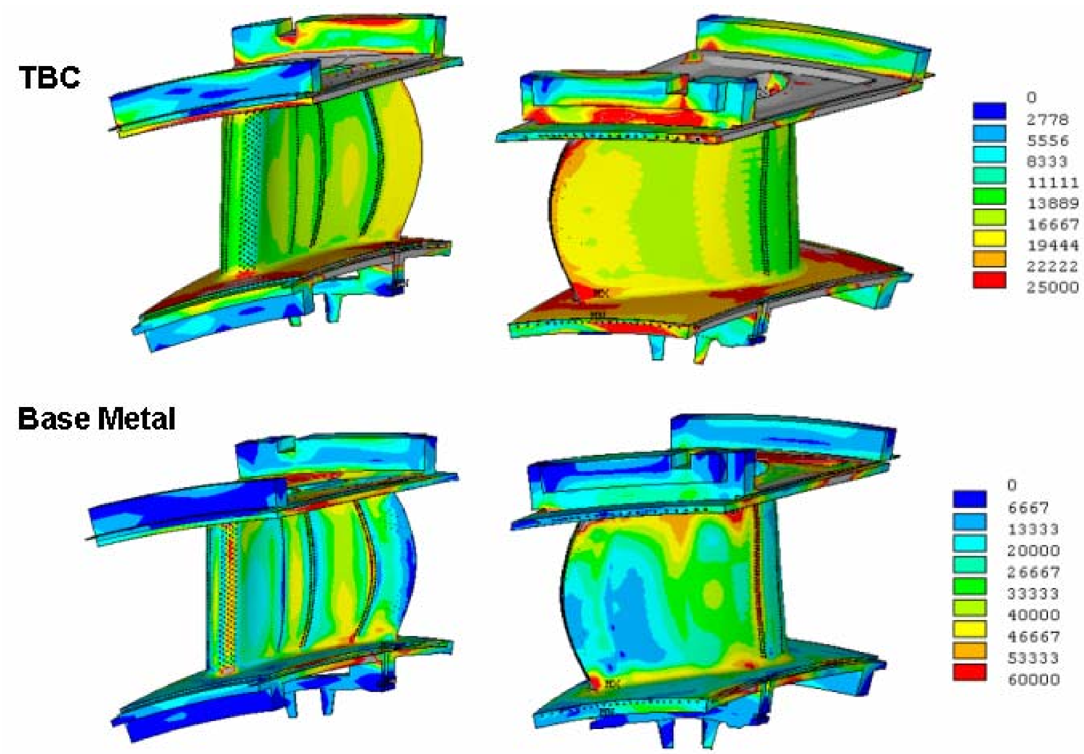

Figure 5-1
Equivalent Stress Distribution of 1^{st} Stage Nozzle

In the ceramic topcoat, tensile stress was generated due to differential thermal expansion between the base metal and the TBC. However, the tensile stress found in the plane perpendicular to the TBC and bond coat interface may actually not pose a reliability issue due to a large degree of strain tolerance within the ceramic topcoat. In general, a TBC is supposed to result in more moderate base metal temperatures and stresses. Nevertheless, for machines that see a significant number of duty cycles, bond coat cracking may occur before the TBC spalls, due to thermally induced high stresses at the interface with the base metal when a cycle is completed. It is also imperative to the overall structure that the TBC remains intact. Loss of the ceramic topcoat could allow the metal temperature to increase as much as 350º F (177º C), thereby allowing for significant oxidation of the base material that is no longer protected.

Figure 5-2 and **Figure 5-3** depict the radial stress and minimum principal stress distributions in the base metal. These show how compressive stress is produced near the external metal surfaces as a result of the hotter outer surface and colder inner surface during base load operation.

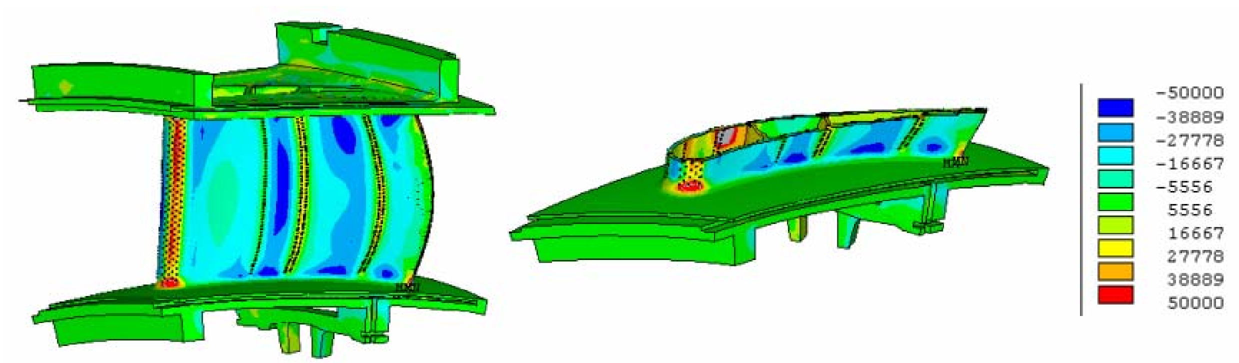

Figure 5-2
Radial Stress Distribution in Base Metal

An appreciable compressive radial stress of about 50 ksi was calculated on the pressure side at the junction of the vane and inner shroud region (**Figure 5-2** and **Figure 5-3**). High localized stress is predicted near the hub of the three cavities, with the strongest stress concentration near the 3rd cavity. The resulting stress pattern can be directly associated with the thermal gradient across the wall and along the fillet radii. The geometric transition from the airfoil to the shroud further contributes to the overall stress created at the inner shroud-fillet region.

Notably, the predicted stress distribution was consistent with the location of major cracks that have occurred on 1st stage nozzles. Another correlation between the predicted stress pattern and inspections of serviced parts is found on the suction side at the inner fillet radii shown in **Figure 5-3**.

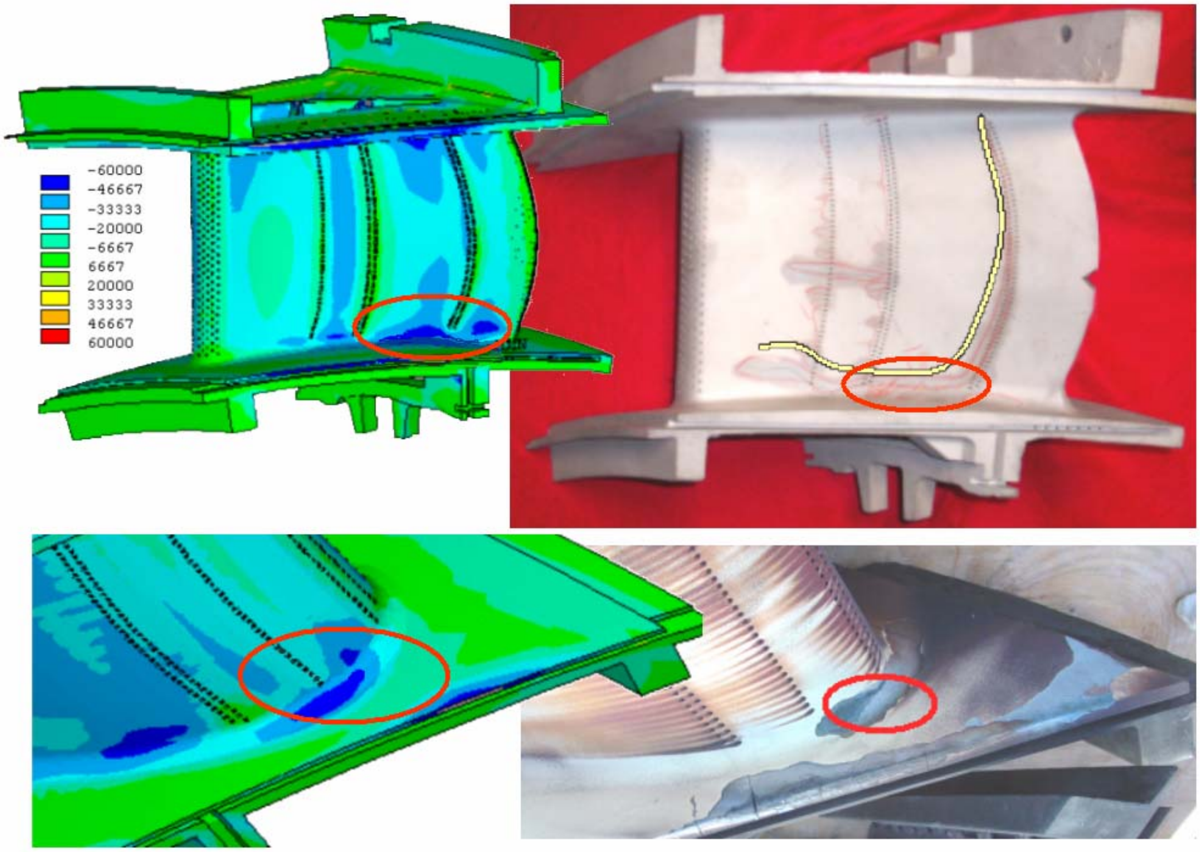

Figure 5-3
Minimum Principal Stress Distribution of Base Metal

Although not evaluated at this time, additional tensile stresses are to be expected during the transient changes in heating and cooling that occur from shutdown and trip events. As such they may also be anticipated to contribute to both crack initiation and propagation. The steady state calculations demonstrate that the aero thermal and structure models are capable of capturing the characteristics and behavior of the 1st stage nozzle with a complex design and a TBC system. However, the additional effort required to perform transient aero-thermal and stress analyses for various thermal cycles to predict TMF life prediction for crack initiation will be substantial.

For rotating components, pursuit of the transient cases are necessary to provide a basis for tracking the accumulation of damage and offer an alternative estimate of overall life consumption on a cycle-by-cycle basis. Because failure of a rotating component would be catastrophic, crack initiation or coating depletion (causing the exposure of base metal) is used as a conservative basis to project inspection and replacement intervals for these hot section components. [8]

Different from their rotating counterparts, life management of the 1st stage nozzles are more likely to hinge upon the time associated with crack propagation or coating erosion, rather than the cycles leading to crack initiation. In other words, because they are stationary, they have a much greater tolerance for initial damage than the highly loaded and stressed blades. From a life cycle management perspective, rather than tracking damage on these components, the aero thermal model currently developed would be more suited to identify and quantify localized design improvements and/or repairs to extend present refurbishment applications.

More in line with the process of root cause investigation versus design life prediction, the computer model is first correlated against field evidence of cracking or other forms of damage. Next, stress and temperatures are calibrated for the critical location(s) where cracks develop. Finally, the model is exercised to investigate changes in proposed changes to structure, materials or cooling. A comparison of results before and after provides a basis to assess the merits (and costs) of alternatives for correcting the root sources or causes of the cracking. In this manner a deliberate solution is engineered, and a trial and error approach is avoided.

Already practiced on a limited basis to guide in the repairs of several F-class rotating components, the aero thermal and structural models of stationary components life the S501FC nozzle would be ideally suited to further serve in this capacity.

6 CONCLUSIONS

1. An aero thermal model was developed for the S-W 501FC 1st stage nozzle. It proved capable of benchmarking the temperatures and stress that result during normal base load operation. A rigorous approach to modeling, previously used on rotating components, was successfully adopted to simulate the more complicated cooling configuration of this F-class stationary hot section component. A workable finite element mesh was designed to include all 767 holes in the vane, inner shroud and outer shroud segments to accurately reflect their role in the subsequent aero thermal and structural analyses.

2. The air flow test performed on all three cavities under various supply pressure levels was significantly more controlled than similar tests performed earlier on first stage buckets. The consequence was evident in the good-to-excellent correlation with results from each of the separate cavities. Given the extremely complex cooling flow strategy that is comprised within an F-class type of nozzle, the results provided significant assistance in representing the cooling flow through the extremely complex passages and schemes used to keep the overall nozzle from overheating. Not only did they provide a basis to verify the cooling flow model, but they also guided its refinements and adjustments. Since an accurate prediction of the internal cooling is the first fundamental layer forming the overall aero thermal and structural analysis, the ability to verify this aspect allowed the program to proceed with a high degree of confidence.

3. Moderate bulk metal temperatures around 1500 ºF (816 ºC) were calculated throughout most of the airfoil portion of the nozzle. By employing several advanced methods to direct the cooling flow in conjunction with a TBC system, the benchmark results show these strategies effectively cool most of the 1st stage vane. It is likely that the average metal temperatures of the 501F design are comparable or possibly even lower than those of the preceding 501D design.

4. Although the overall bulk metal temperature appears to be moderate considering the extremely high gas temperature environment localized high temperature gradients were still present, particularly in the regions comprising the side wall fillet and shroud. These locations where high temperature gradients occur are natural candidates for high stress, which can lead to cracking from repeated thermal cycles.

5. Considerably high temperatures and temperature gradients were found at the inner fillet of pressure side, near the hub region of 3rd cavity. Surface metal temperature at this location was predicted to be around 1700º F (927º C). It appears that the primary failure mechanism of critical inner fillet cracking is not likely caused by time-dependent high temperature

oxidation. Instead, cracking in the inner fillet is more likely associated with thermal stress induced from a high temperature gradient caused by repeated thermal cycling.

6. Compressive stresses were produced near the external metal surfaces as a result of the difference caused between the hotter outer surface and colder inner surface. In the ceramic topcoat, tensile stress was generated due to differential thermal expansion between the base metal and the TBC. Stresses in the topcoat TBC 20 ksi are lower than in the vane section. A higher stress of about 25 ksi was calculated on the topcoat in the inner shroud region. Tensile stress in the plane perpendicular to the TBC and bond coat interface might may not be a threat due to a large degree of strain tolerance of ceramic top coat.

7. In general, the results demonstrate how a TBC moderates the base metal temperature and stresses. However, for machines that see a number of cycles between inspection internals, cracking of the bond coat cracking may occur before the more traditional failure of a TBC by delaminating and spalling. For a machine that primarily operates at base load, it is imperative in terms of nozzle durability that the TBC remains intact. If the TBC is compromised with loss of the ceramic topcoat, the base metal could see a temperature increase of up to 350 ºF, resulting in severe oxidation.

8. An appreciable compressive radial stress of about 50 ksi was calculated on the pressure side at the junction of vane and inner shroud region. Localized stresses were also predicted near the hub of the three cavities with the highest stress concentration present near the 3rd cavity. The resulting stress patterns appear to be associated with a thermal gradient across the wall and along the fillet radii. The geometric transition from airfoil to shroud further contributes to the overall stress level at the inner shroud-fillet region. The distribution of stress appears consistent with a major form of cracking that has occurred on 1st stage nozzles of this design.

9. The tensile stresses produced during shutdown and trip events are also expected to contribute to both crack initiation and propagation in this location, although this was not pursued in the steady state examination. However, the base load applications demonstrates that the aero thermal and structural models are capable of capturing the transient thermal characteristics and behavior of hot section parts that have a complex design and a TBC system. Pursuing transient aero-thermal and stress analyses for various thermal cycles could similarly process TMF life prediction for crack initiation in the 1st stage nozzles. The efforts required to conduct these transient analyses will be substantially greater than for blades because of the significantly more complicated internal cooling strategies involved with stationary nozzles.

10. Since the life management of the 1st stage nozzle is much more likely to depend upon the role of crack propagation, rather than crack initiation, which is used as a conservative limit to mark the safe operating life of a rotating component, the need for pursuing transient studies should be weighed differently than when rotating parts are assessed. Recognizing that much more of the total life may still be associated with crack propagation before final rupture of pieces from the nozzle occurs, the aero thermal model currently developed might be better applied to evaluate design improvements or repairs associated with refurbishments beyond the limits allowed by the OEM. In other words, because this is a stationary component, the value of a durability analysis and benchmarking the aero thermal and structural properties of

such a design are more likely to be in supporting repair and/or inspections efforts rather than in regularly tracking the accumulation of damage.

11. The success in obtaining a numerical solution implies that a transient analysis is certainly feasible, although repeating the single sequence of steps performed in the base load analysis is not without different challenges. Effectively transferring the tremendous amounts of information will require addition attention to ensure the iteration scheme correctly handles the time-steps of the start-up or shutdown of the cycle.

12. Similar to what has been done on the SW 501FC 1st stage bucket, the benchmark model can guide non-standard or non-OEM repairs by provide a basis to evaluate proposed localized changes in structure and cooling. The changes in temperatures and stresses are compared before and after, and used to qualitatively assess the merits of the changes. In regard to inspection and damage limits, the benchmark model may also provide a basis to further evaluate the consequence of cracks that are known to develop in critical locations based on historical experience. In these locations, the original model would be modified with crack elements to assess their potential for failure as they extend or grow in through the airfoil.

7
SUMMARY REMARKS

1. *What do the results suggest in terms of increasing the durability of the present design?*

   The major cracking problem appears to be in the fillet region between the inner shroud and vane, approximate to the 3rd cavity. The results indicate that this is primarily a cooling issue. In other words, strengthening the fillet or improving the coating is not likely to inhibit the development of cracks.

2. *How might the inner shroud-fillet cracking be approached?*

   Similar to what was done in the upper shroud, reduction of the thermal gradient requires some type of impingement (film) cooling strategy. An examination of the 3rd cavity reveals how the impingement cooling holes down the vane are already extended as far as possible into this region, but still are unable to provide sufficient relief in terms of mitigating the thermal gradient that is caused by the differential expansion of the material as it transitions from the fillet to the thin surface of the vane.

3. *Why not apply the same film cooling strategy used on the outer shroud?*

   The design problem associated with the addition of impingement cooling to the lower shroud is that the pressure is much lower in contrast to the pressures that feed the film cooling of the upper shroud. A corrective strategy therefore involves more than simply adding more cooling holes. The pressures must also be sufficient to serve the holes by the time the flow reaches the inner shroud. Cooling relieves the gradient, but there is only so much flow available to cool the nozzle.

4. *Why not simply strengthen this region?*

   This is not just an issue of stress, but of the thermal gradient that is caused because of the differences in localized thicknesses and the differential thermal expansion rates that are produced. If more material is added to enlarge the fillet region, the crack would only move toward the weakest edge where the fillet meets the thin wall of the vane. Reducing the fillet and it may not have the strength to profide sufficient rigidity and support.

5. *How reliable are the results produced from this initial application to a nozzle?*

   As emphasized throughout the report, the aero thermal analysis of the first stage nozzle used in an F-class unit represents the leading edge of technical complexity undertaken to date in the overall EPRI hot section initiative. A highly complicated geometry and internal cooling scheme creates enormous amounts of information, which must be systematically transferred between the cooling and structural model in order to produce a reasonably accurate profile of temperaturs and stress. The correlation with both the airflow test results and limited field experience indicates the results are certainly reasonable enough to serve the purpose of the EPRI initiative, i.e. to remove the "black box" between the design and response of these components.

6. *How important is it to the nozzle that the integrity the TBC is maintained?*

   An example of removing the "black box" mentioned in the previous comment is shown by the calculation of the metal temperatures of the nozzle with the TBC in place. With the TBC, the base metal temperatures in the nozzle are about 1750°F (954°C). Without the TBC the temperatures would go up to around 1950°-2000°F (1066°-1093°C). At this temperature the metallic coating would oxidize quickly. Evidence of this is the local oxidation that was apparent in the field serviced parts where the TBC had eroded or spalled off.

7. *What are the limitations of the TBC?*

   At the operating temperatures which the 1st stage is exposed to, a TBC is absolutely necessary. In fact it is the TBC (in addition to the internal and impingement cooling) that makes it possible to run at these higher temperatures for any length of time. But improvements in coatings, like the other engineering strategies employed on hot section components, are being pushed to the edge of the envelop in the competition to produce more power and better thermal efficiency.

8. *Should damage tracking of the nozzle be pursued in the same way as for blades?*

   For both blades and nozzles the goal of the HSLMP remains to <u>predict</u> damage. To use the results of the nozzle study however, a distinction should be made that was clearly evident in the field serviced parts used to correlate against the predicted results. For blades, safe operating life is considered the point when cracks *initiate*. For nozzles however, life is measured by the rate of crack *propagation*. It is further believed that cracks formed in the nozzle may initiate very early in the operating history, at locations like the shroud fillet. The approach to approximate damage which is applied to the rotating components would therefore necessarily focus on calibrating useful life in terms of propagation versus initiation. To assess crack propagation necessarily requires an additional step involving fracture mechanics, not typically performed to independently assess life consumption in rotating components.

9. *Should damage accumulation in nozzles be tracked?*

   Distinctive from blades, nozzles do not experience the combined centrifugal and vibratory forces that can lead to a catastrophic failure relatively soon after a crack is formed. They therefore do not represent the same potential consequence in terms of damage to the machine, should portions of the component to be liberated while still in service. It is also likely that blade life consumption (oxidation, TMF, creep) will continue to dominate and control the intervals that are set for F-class hot gas paths. The inspection intervals that the blades force will continue to allow the nozzles to be inspected for the appearance of cracks.

10. *Should the transient analysis be completed?*

    As stated in the report, with the successful completion of a steady state analysis, the transient analysis is considered feasible. With rotating components, it would be the logical next step to profile the response during events such as start-up, shutdown, trips, etc. in order to calibrate the damage caused by TMF. However, such a calculation would represent another milestone in terms of technical challenge, because the enormous amount of data transferred to complete the steady state analysis will need to be accomplished for each time step increment of the transient. This could increase the number of calculations by 15-20 times per event.

References

1. H. L. Bernstein, R. C. McClung, T. R. Sharron and J. M. Allen, "*Analysis of General Electric Model 7001 First Stage Nozzle Cracking*", 92-GT-311, 1992.

2. J. Yau and H. Kuang, "*An Empirical Model for Predicting Crack Growth Behavior of Gas Turbine Stage 1 Nozzles*", GT-2002-30302, 2002.

3. T. Fujii and T. Takahashi, "*Study on Crack Propagation Tendencies of Non-repaired and Repaired Nozzles*", GT-2003-38351, 2003.

4. A. Scalzo, et al. "*A New 150MW High Efficiency Heavy-Duty Combustion Turbine Combustion Turbine*", 88-GT-162, 1988.

5. G. Kumar, et al. "*A Generalized One Dimensional Computer Code for Turbomachinery Cooling Passage Flow Calculations*", AIAA 89-2574, 1989.

6. R. V. Chima, "*Explicit Multigrid Algorithm for Quasi-Three-Dimensional Viscous Flows in Turbomachinery,*" AIAA Journal of Propulsion and Power, Vol. 3 No. 5, 1987.

7. R. J. Boyle and F. F. Simon, "*Mach Number Effects on Turbine Blade Transition Length Prediction*", Journal of Turbomachinery, Vol. 121, 1999.

8. EPRI 10004364 "Combustion Turbine F-Class Life Management – Maintenance Life Tracking, December 2002.

The Electric Power Research Institute (EPRI)

The Electric Power Research Institute (EPRI), with major locations in Palo Alto, CA, and Charlotte, NC, was established in 1973 as an independent, non-profit center for public interest energy and environmental research. EPRI brings together member organizations, the Institute's scientists and engineers, and other leading experts to work collaboratively on solutions to the challenges of electric power. These solutions span nearly every area of power generation, delivery, and use, including health, safety, and environment. EPRI's members represent over 90% of the electricity generated in the United States. International participation represents over 10% of EPRI's total R&D program.

Together…shaping the future of electricity

Export Control Restrictions
Access to and use of EPRI Intellectual Property is granted with the specific understanding and requirement that responsibility for ensuring full compliance with all applicable U.S. and foreign export laws and regulations is being undertaken by you and your company. This includes an obligation to ensure that any individual receiving access hereunder who is not a U.S. citizen or permanent U.S. resident is permitted access under applicable U.S. and foreign export laws and regulations. In the event you are uncertain whether you or your company may lawfully obtain access to this EPRI Intellectual Property, you acknowledge that it is your obligation to consult with your company's legal counsel to determine whether this access is lawful. Although EPRI may make available on a case by case basis an informal assessment of the applicable U.S. export classification for specific EPRI Intellectual Property, you and your company acknowledge that this assessment is solely for informational purposes and not for reliance purposes. You and your company acknowledge that it is still the obligation of you and your company to make your own assessment of the applicable U.S. export classification and ensure compliance accordingly. You and your company understand and acknowledge your obligations to make a prompt report to EPRI and the appropriate authorities regarding any access to or use of EPRI Intellectual Property hereunder that may be in violation of applicable U.S. or foreign export laws or regulations.

1011622

Printed on recycled paper in the United States of America

Electric Power Research Institute (EPRI) • 3412 Hillview Avenue, Palo Alto, California 94304 • PO Box 10412, Palo Alto, California 94303 • USA
800.313.3774 • 650.855.2121 • askepri@epri.com • www.epri.com